

Throat effects on strong gravitational lensing in Kerr-like wormholes

Tien Hsieh, Da-Shin Lee,^{*} and Chi-Yong Lin[†]

*Department of Physics, National Dong Hwa University,
Hualien 97401, Taiwan, Republic of China*

(Dated: September 27, 2024)

Abstract

We study the strong gravitational lensing by the Kerr-like wormholes with an additional parameter to specify the location of the throat. We classify the roots of the radial potential derived from the null geodesic equations. We focus on the throat together with other roots to become either double root or triple root, potentially giving the divergence of the deflection angle of the light rays in the strong deflection limit (SDL). In particular, while the logarithmic divergence is known as the double roots are approached, the more stronger power-law (non-logarithmic) divergence is found for the triple roots. In addition, the effective potential in terms of the proper distance from the throat is constructed with which to realize how the light rays can either travel within one spacetime, where the observers are located or pass through the throat into another spacetime, where different observers reside. The observational effects, such as relativistic images resulting from the deflection of light by wormholes, are discussed.

PACS numbers: 04.70.-s, 04.70.Bw, 04.80.Cc

^{*}Electronic address: dslee@gms.ndhu.edu.tw

[†]Electronic address: lyong@gms.ndhu.edu.tw

I. INTRODUCTION

Wormholes are hypothetical spacetime that connect two separate regions of the universe or even different universes. These hypothetical structures in spacetime are solutions to Einstein's equations of general relativity [1]. Einstein and Rosen introduced a mathematical construction in order to eliminate coordinate or curvature singularities with a bridge-like structure known as the Einstein-Rosen bridges [2]. Later Wheeler interpreted the Einstein-Rosen bridge as a link between distant points in spacetime and then coined the term wormhole, albeit on the small scales [3, 4]. Traversable wormholes were proposed by Morris and Thorne [5], allowing observers on a human scale to freely traverse them. Since then, numerous publications have explored all sorts of wormholes, but they all have shared the thing in common of violating the energy condition, at least in a neighborhood of the wormhole throat. For a review, see [6]. While exotic stabilization schemes have been proposed, there is currently no evidence that wormholes exist.

Einstein's century-old prediction as a consequence of general relativity (GR) has been confirmed by recent detection of gravitational waves emitted from the merger of binary black holes system [7–9]. The capture of the spectacular images of a supermassive black hole M87* at the center of M87 galaxy [10] and Sgr A* at the center of our galaxy [11] provide further important scientific evidence directly confirming the existence of black holes. Gravitational lensing is the other powerful tool to test GR [1, 12] from strong field perspectives [13–23]. In particular, in [21–23], we have studied the gravitational lensing and time delay by a spinning charged black hole. Damour and Solodukhin were the first to propose the Schwarzschild-like wormhole [24], where the gravitational lensing was studied in the strong deflection limit (SDL) [25, 26]. Following the same construction, Kerr-like wormholes were also proposed. The throat effects have been extensively explored on the shadow image and echo [27–29]. Here we will focus on the gravitational lensing by the Kerr-like wormholes. The results will be compared to the Kerr black holes in [22], so that we can tell the difference between the wormholes and the black holes based on their lensing effects in the SDL.

The study of the lensing effects due to the wormholes can be examined as illustrated in Fig. 1. The light rays are emitted from the source, and circle around the wormholes multiple times in the SDL along a direct orbit (red line) or a retrograde orbit (blue line), giving two sets of the relativistic images. However, a unique feature of wormholes is that, for certain

parameters of light rays, they can pass through the throat and reach another spacetime from the spacetime of the light source. When the observers are in the same spacetime of the light sources, the observers will see the light fall into the throat to another spacetime with the trajectory in Fig. 1 from the light sources to the throat. When the light sources are in the different spacetime from the observers, the observers will see the light rays come out and reach them from the throat to the observers. Due to the symmetry of the proper distance l measured from the throat, which will be defined later, namely $l \rightarrow -l$, one can map the light rays from the sources from another spacetime to the spacetime of the observers. This type of the trajectories of the light traveling between two spacetimes can be visualized in Fig. 6 in [30]. Thus, according to [31] the same lens equation is assumed as in the cases when the observers and the light sources are in the same spacetime. In the future work, we will extend the work of [30] to find the detailed trajectories of the light rays to further depict the light deflection around the wormholes in one spacetime or between two spacetimes given in what we called embedded diagram in Fig. 2. Following the approach of [22] enable us to study the observational consequences.

Layout of the paper is as follows. In Sec. II, we first introduce the Kerr-like wormholes. Then, we give a brief review of the equations for the null geodesics, mainly focusing on the equatorial orbits, from which the radial potential can be defined in terms of its roots. Thus, the effective potentials, as a function of the coordinate r and the proper distance l , respectively, are constructed to clearly show the types of light deflection under investigation. Sec. III is devoted to the study of the strong field limit, where the throat of the wormholes together with other roots of the radial potential become the double or triple roots, giving the divergence of the deflection angle as the roots are approached. In Sec. IV, the deflection angle in the weak field limit is also studied when the turning point is far from the throat. The relativistic images of gravitational lens, leading to observational effects are discussed in Sec. V. In Sec. VI, we summarize the main results and discuss the perspectives. Appendix A is added for summarizing the roots of the radial potential of the Kerr black holes, which are also the roots of the radial potential of the Kerr-like wormholes.

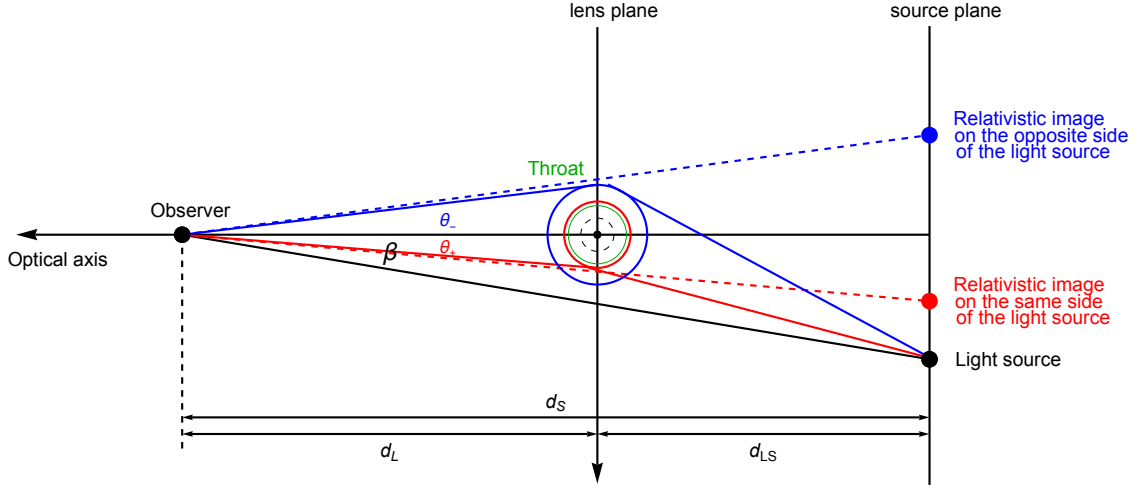


FIG. 1: Gravitational lens about relativistic images when the observers and the light sources are in the same spacetime. Considering the Kerr-like wormholes with angular momentum of the clockwise rotation, the light rays are emitted from the source, and circle around the black hole multiple times in the SDL along a direct orbit (red line) or a retrograde orbit (blue line). The graph illustrates two sets of the relativistic images. When the observers and the light sources are in the different spacetime, mapping the light rays in the spacetime of the sources to that of the observers in terms of the proper distance from the throat l through $l \rightarrow -l$ will expect to see the same lens diagram above (for example, see Fig. 6 of [30]). See also the main text for details.

II. KERR-LIKE WORMHOLES AND THE DEFLECTION ANGLE

We first introduce the Kerr-like wormhole metric with which to consider the deflection angle $\hat{\alpha}(b)$ of light rays for a given impact parameter b , in particular in the SDL. The metric of the Kerr-like wormhole is constructed by an additional parameter λ characterizing a throat r_{th} from that of the Kerr black hole with a family of the parameters of the gravitational mass M , and angular momentum per unit mass $a = J/M$, which reads, in Boyer-Lindquist coordinates, as [28]

$$\begin{aligned}
 ds^2 &= g_{\mu\nu} dx^\mu dx^\nu \\
 &= - \left(1 - \frac{2Mr}{\Sigma} \right) dt^2 - \frac{2Mar \sin^2 \theta}{\Sigma} (dt d\phi + d\phi dt) \\
 &\quad + \frac{\Sigma}{\Delta} dr^2 + \Sigma d\theta^2 + \left(r^2 + a^2 + \frac{2Ma^2 r \sin^2 \theta}{\Sigma} \right) \sin^2 \theta d\phi^2, \tag{1}
 \end{aligned}$$

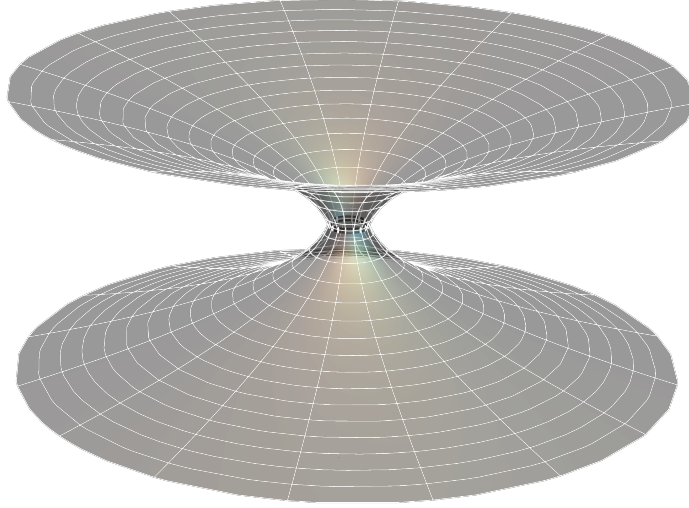


FIG. 2: Embedding diagram of the Kerr-like wormhole with $a = 0.5$ and $\lambda = 0.3$ from [29]. The upper spacetime corresponds to the proper radial distance $l > 0$ while the lower one corresponds to the proper radial distance $l < 0$. The thinnest place between the two spacetimes is the throat with $l = 0$ in (18).

where

$$\begin{aligned}\Sigma &= r^2 + a^2 \cos^2 \theta, \\ \hat{\Delta} &= r^2 + a^2 - 2M(1 + \lambda^2)r = (r - r_{\text{th}})(r - \tilde{r}_-), \\ \Delta &= r^2 + a^2 - 2Mr = (r - r_+)(r - r_-),\end{aligned}\tag{2}$$

and the deviation parameter $\lambda \geq 0$ in general. The radius of the throat can be obtained by solving $\hat{\Delta}(r) = 0$, giving

$$r_{\text{th}} = M(1 + \lambda^2) + \sqrt{M^2(1 + \lambda^2)^2 - a^2},\tag{3}$$

and another root is

$$\tilde{r}_- = M(1 + \lambda^2) - \sqrt{M^2(1 + \lambda^2)^2 - a^2}.\tag{4}$$

The Schwarzschild-like wormhole in [24] can be reduced by setting $a = 0$. However, in the case of $\lambda = 0$ corresponding to the Kerr black holes, $\hat{\Delta} \rightarrow \Delta$ with the outer (inner) horizon r_+ (r_-) given by

$$r_{\pm} = M \pm \sqrt{M^2 - a^2}\tag{5}$$

and the condition $M^2 > a^2$. Additionally, the ADM mass of the wormhole can be computed to be [29]:

$$M_{\text{WH}}^{(\text{ADM})} = M(1 + \lambda^2) \quad (6)$$

as seen by an observer at the asymptotic spatial infinity.

For this asymptotically flat, stationary, and axial-symmetric spacetime, where the metric is independent of t and ϕ , there exist the conserved quantities, namely the energy ε and the azimuthal angular momentum ℓ along a geodesic, which can be constructed by the Killing vectors and the 4-velocity $u^\mu = dx^\mu/d\sigma \equiv \dot{x}^\mu$ in terms of the affine parameter σ as

$$\varepsilon \equiv -\xi_t^\mu u_\mu, \quad \ell \equiv \xi_\phi^\mu u_\mu. \quad (7)$$

The associated Killing vectors are given by:

$$\xi_t^\mu = \delta_t^\mu, \quad \xi_\phi^\mu = \delta_\phi^\mu. \quad (8)$$

Here, we focus on the light rays traveling in the equatorial plane of the wormhole, namely $\theta = \pi/2$ and $\dot{\theta} = 0$. Thus, together with the null geodesics, where $u^\mu u_\mu = 0$, the equations of motion in the Boyer-Lindquist coordinates can be written as the first-order differential equations

$$\frac{\Sigma}{\varepsilon} \frac{dr}{d\sigma} = \pm_r \sqrt{\tilde{R}(r)}, \quad (9)$$

$$\frac{\Sigma}{\varepsilon} \frac{d\phi}{d\sigma} = \frac{a}{\Delta} (r^2 + a^2 - ab_s) + b_s - a, \quad (10)$$

$$\frac{\Sigma}{\varepsilon} \frac{dt}{d\sigma} = \frac{r^2 + a^2}{\Delta} (r^2 + a^2 - ab_s) + a(b_s - a) \quad (11)$$

with $\Sigma = r^2$ on the equatorial plane. In these equations, we have introduced the impact parameter

$$b_s = s \left| \frac{\ell}{\varepsilon} \right| \equiv s b \quad (12)$$

with $s = \text{Sign}(\ell/\varepsilon)$ and b being a positive magnitude. The parameter $s = +1$ for $b_s > 0$ is referred to as direct orbits, and those with $s = -1$ for $b_s < 0$ as retrograde orbits (see Fig. 1 for the sign convention). The radial potential of a Kerr-like wormhole is obtained as

$$\tilde{R}(r) = \frac{(r - r_{\text{th}})(r - \tilde{r}_-)}{(r - r_+)(r - r_-)} R(r) \quad (13)$$

with the radial potential $R(r) = (r - r_1)(r - r_2)(r - r_3)(r - r_4)$, solely depending on the mass M and the spin a , which is the same as the radial potential of Kerr black holes with

four roots ($r_1 < r_2 < r_3 < r_4$) in Appendix [32] when the roots are all real valued. Notice that $r_2 = 0$ on the equatorial plane.

To find the closest distance of the light rays r_0 , we start from solving the radial potential $\tilde{R}(r_0) = 0$, and then the condition leads to two results, $r_0 = r_{\text{th}}$ and $R(r_0) = 0$. The former means that light rays will reach the throat, fall into the wormhole, and then travel to another spacetime; the latter is that the outermost root r_4 is a turning point r_0 of the light rays coming from the spatial infinity with the value given by

$$r_0(b) = 2\sqrt{\frac{1}{3}(b^2 - a^2)} \cos \left\{ \frac{1}{3} \cos^{-1} \left[\frac{-a^2M + 2Msab - b^2M}{\left(\frac{b^2 - a^2}{3}\right)^{3/2}} \right] \right\}, \quad (14)$$

which can be obtained from $R(r_0) = 0$ or (A7) in Appendix by rewriting it in a form of trigonometric functions. One also can obtain the impact parameter as

$$b(r_0) = \frac{2sMa - r_0\sqrt{a^2 - 2r_0M + r_0^2}}{2M - r_0}. \quad (15)$$

In addition, another type of potential that is more commonly used is the effective potential defined below. The equation of motion along the radial direction can be cast in the form [21]

$$\frac{1}{b^2} = \frac{\dot{r}^2}{\ell^2} + W_{\text{eff}}(r), \quad (16)$$

from which to define the effective potential W_{eff} as

$$W_{\text{eff}}(r) = \left[1 - \frac{(r - r_{\text{th}})(r - \tilde{r}_-)}{(r - r_+)(r - r_-)} \right] \frac{1}{b^2} + \frac{(r - r_{\text{th}})(r - \tilde{r}_-)}{(r - r_+)(r - r_-)} \frac{1}{r^2} \left[1 - \frac{a^2}{b^2} - \frac{2M}{r} \left(1 - \frac{sa}{b} \right)^2 \right]. \quad (17)$$

We now introduce the proper radial distance l connecting two spacetimes by

$$\begin{aligned} l &\equiv \pm \int_{r_{\text{th}}}^r \sqrt{\frac{\Sigma}{\hat{\Delta}}} dr \\ &= \sqrt{r^2 + a^2 - 2M(1 + \lambda^2)r} + M(1 + \lambda^2) \log \left(\frac{\sqrt{M^2(1 + \lambda^2)^2 - a^2}}{r - M(1 + \lambda^2) - \sqrt{r^2 + a^2 - 2M(1 + \lambda^2)r}} \right), \end{aligned} \quad (18)$$

where the value of l can be extended to $-\infty < l < \infty$, and the throat is located at $l = 0$. In Fig. 2, the embedded diagram of the Kerr-like wormholes on the equatorial plane is drawn from [29], where $l > 0$ corresponds to one spacetime and $l < 0$ for another spacetime. Then, (16) can be rewritten in terms of the proper radial distance l as

$$\dot{l}^2 + \varepsilon^2 w_{\text{eff}}(l) = 0 \quad (19)$$

with w_{eff} given by

$$w_{\text{eff}}(l) = \frac{4Msab + b^2[r(l) - 2M] - a^2[2M + r(l)] - r^3(l)}{r(l)[a^2 + r^2(l) - 2Mr(l)]}, \quad (20)$$

where the effective potential $w_{\text{eff}}(l)$ proves to be very useful to realize the various types of the light deflection for a given set of the light ray parameters and the location of the throat discussed below.

Solving the differential equation obtained from (9) and (10)

$$\frac{dr}{d\phi} = \frac{\sqrt{(r - r_+)(r - r_-)(r - r_{\text{th}})(r - \tilde{r}_-)R(r)}}{br(r - 2M) + 2Msar} \quad (21)$$

gives the deflection angle $\hat{\alpha}$ defined by

$$\hat{\alpha} + \pi = 2 \int_{r_0}^{\infty} \frac{br(r - 2M) + 2Mar}{\sqrt{(r - r_+)(r - r_-)(r - r_{\text{th}})(r - \tilde{r}_-)R(r)}} dr. \quad (22)$$

In the next section, we will calculate the deflection angle using this formula in the SDL.

III. DEFLECTION ANGLE IN THE STRONG DEFLECTION LIMIT

In general, the parameter of the light ray $b(r_0)$ can be arbitrary. As r_0 gets closer to the double or triple root of the radial potential $\tilde{R}(r)$, defined as the critical distance r_c with the corresponding impact parameter b_c , the deflection angle increases and even diverges. In the case of black holes, it is known that the impact parameter is restricted to $b > b_c$ determined by the double roots of the outermost two roots $r_3 = r_4$ [21, 33]. Otherwise, when $b < b_c$, the light rays will be pulled into black holes. In wormholes with the presence of the throat characterized by λ , apart from the double roots of $r_3 = r_4$, there might exist another double root, namely $r_4 = r_{\text{th}}$ shown in Fig. 3. All double roots might merge to form a triple root $r_3 = r_4 = r_{\text{th}}$, say, at λ_c and b_c also shown in Fig. 3. Therefore, one can have the respective parameter regions of the double roots of $r_3 = r_4 < r_{\text{th}}$ for $\lambda < \lambda_c$ and $r_3 = r_4 > r_{\text{th}}$ for $\lambda > \lambda_c$ with the impact parameter b_c [21, 33].

With a fixed value $\lambda < \lambda_c$, for $b > b_c$, the turning point lies in $r_0 = r_4$, and for $b = b_c$, the turning point becomes $r_0 = r_4 = r_3$. But for $b < b_c$, no turning point exists outside the throat, since r_3 and r_4 are complex conjugate roots and thus the light rays pass through the throat to another spacetime from the spacetime of the light sources. The above trajectories of light rays become clear from the graphs of the effective potential $W_{\text{eff}}(r) - 1/b^2$ and $w_{\text{eff}}(l)$

in Figs. 4 and 5, respectively. The deflection angle due to the double roots of $r_3 = r_4$ as $b \gtrsim b_c$ has a form in the SDL as

$$\hat{\alpha}(b) \approx -\bar{a} \log\left(\frac{b}{b_c} - 1\right) + \bar{b} + O(b - b_c) \log(b - b_c) \quad (23)$$

with two parameters \bar{a} and \bar{b} as a function of the wormhole's parameters. In contrary, along the value of $\lambda = \lambda_c$, and $b = b_c$, $r_0 = r_3 = r_4 = r_{\text{th}}$, a triple root is met with the power-law divergence when $b \gtrsim b_c$ in the SDL as [25]

$$\hat{\alpha}(b) \approx \bar{a} \left(\frac{b}{b_c} - 1\right)^{-1/4} + \bar{b}. \quad (24)$$

For $b < b_c$, light rays will pass through the throat due to the fact that there is no turning point outside the throat, also seen from the graphs of the effective potentials in Figs. 4 and 5. The deflection angle in the SDL can be written in the form for the double root $r_3 = r_4$ as

$$\hat{\alpha}(b) \approx -\bar{a} \log\left(\frac{b_c}{b} - 1\right) + \bar{b} + O(b_c - b) \log(b_c - b) \quad (25)$$

and for the triple root $r_3 = r_4 = r_{\text{th}}$ as

$$\hat{\alpha}(b) \approx \bar{a} \left(\frac{b_c}{b} - 1\right)^{-1/4} + \bar{b}. \quad (26)$$

The existence of the root of r_{th} implies that the light rays can go from $r = \infty$ to $r = r_{\text{th}}$, corresponding to $l = -\infty$ to $l = 0$ from another spacetime of the light ray sources, pass through the throat and then go from $r = r_{\text{th}}$ to $r = \infty$, corresponding to $l = 0$ to $l = \infty$ of the spacetime of the observer. This unique feature of the wormholes can be captured in the effective potentials in Figs. 4 and 5.

Another interesting double root is $r_4 = r_{\text{th}}$ with the critical impact parameter $b(r_{\text{th}}) \equiv b_{\text{th}}$ by (15) for a fixed $\lambda > \lambda_c$ seen in Fig. 3. When $b > b_{\text{th}}$, where $r_4 > r_{\text{th}} > r_3$, the root r_4 serves as a turning point as seen in the plots of the effective potentials. As b approaches to b_{th} from its above, the turning point shifts to the double roots of $r_4 = r_{\text{th}}$, leading to the deflection angle of the divergent form (23) with the critical b_{th} . For $b < b_{\text{th}}$ along the line of $\lambda > \lambda_c$, where $r_{\text{th}} > r_4 > r_3$, there is no turning point, instead the light rays hit the throat r_{th} as an effective light sphere, which is the closest distance of the orbit. Therefore, the SDL deflection angle as $b \rightarrow b_{\text{th}} = b_c$ from the below is given by the same form (25). Finally, in the case of $r_3 = r_4 < r_{\text{th}}$, the presence of the throat leads to a large deflection angle compared to the weak field limit, which will be seen later.

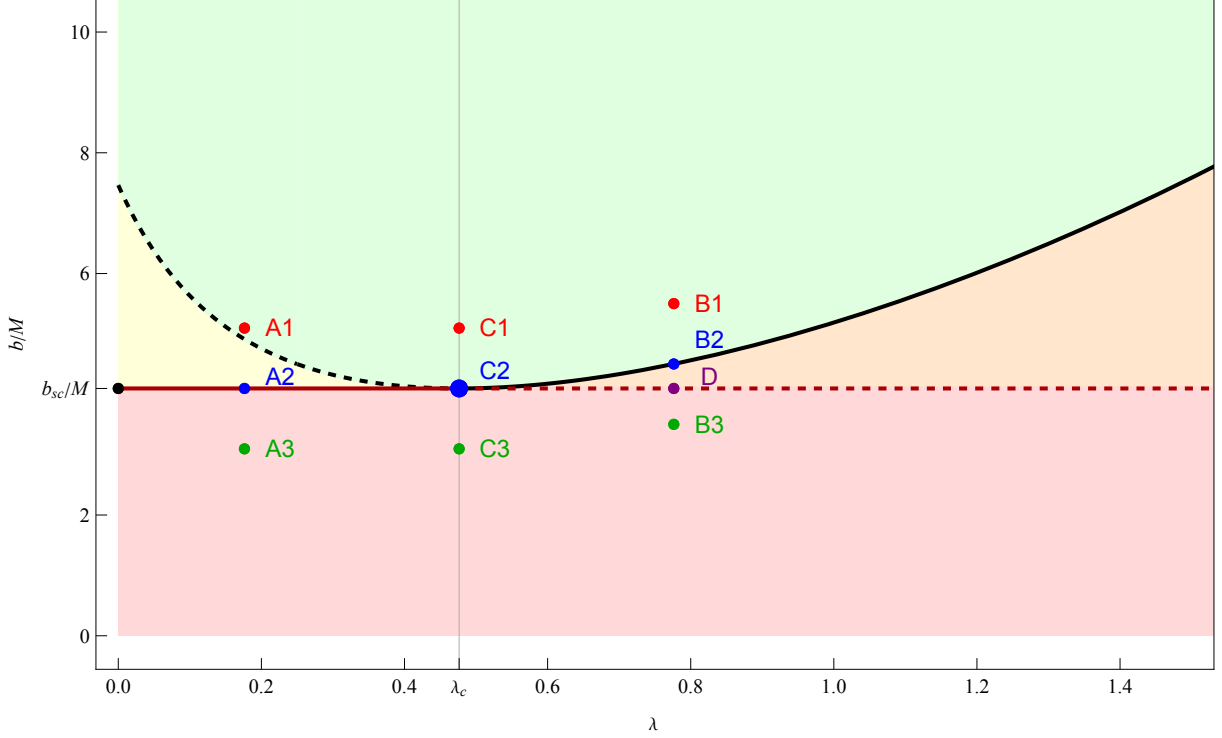


FIG. 3: Diagram of parameter space (λ, b) , where the relevant roots of our study are three outermost roots r_3, r_4 and r_{th} for $a = 0.5$ and $s = +1$ in this illustrative example. The light green, orange, yellow, and red regions correspond, respectively, to the cases $r_4 > r_{\text{th}} > r_3$, $r_{\text{th}} > r_4 > r_3$, $r_4 > r_3 > r_{\text{th}}$, and $r_3 = r_4^*$ and r_{th} , determined by the parameter λ . The red solid (dashed) line is for the double root of $r_3 = r_4 > r_{\text{th}}$ ($r_3 = r_4 < r_{\text{th}}$) with $\lambda < \lambda_c$ and $b = b_{sc}$ ($\lambda > \lambda_c$ and $b = b_{sc}$). The black solid (dashed) line is for the double root of $r_4 = r_{\text{th}} > r_3$ ($r_4 > r_3 = r_{\text{th}}$) with $\lambda > \lambda_c$ and $b = b_{\text{th}}$ ($\lambda < \lambda_c$ and $b = b_{\text{th}}$). Note that λ_c is defined by $r_{\text{th}}(\lambda_c) = r_{sc}$ for a specific wormhole spin a , and the intersection C2 is the triple root. The dots A1, A2, and A3 are along the line of $\lambda < \lambda_c$ in Sec. III A with the respective roots of $r_4 > r_{\text{th}} > r_3$, $r_3 = r_4 > r_{\text{th}}$ and $r_3 = r_4^*$ and r_{th} determined by λ . Furthermore, the black dot at $\lambda = 0$ corresponds to the case of black hole in [22]. The dots C1, C2, and C3 are along the line of $\lambda = \lambda_c$ in Sec. III C with the respective roots of $r_4 > r_{\text{th}} > r_3$, $r_3 = r_4 = r_{\text{th}}$, and $r_3 = r_4^*$ and r_{th} determined by λ . The dots B1, B2, B3, and D are along the line of $\lambda > \lambda_c$ in Sec. III B and III D with the respective roots of $r_4 > r_{\text{th}} > r_3$, $r_4 = r_{\text{th}} > r_3$, $r_3 = r_4^*$ and r_{th} determined by λ , and $r_{\text{th}} > r_4 = r_3$. Note that the light green and yellow regions correspond to the light deflection in the weak field limit in Sec. IV.

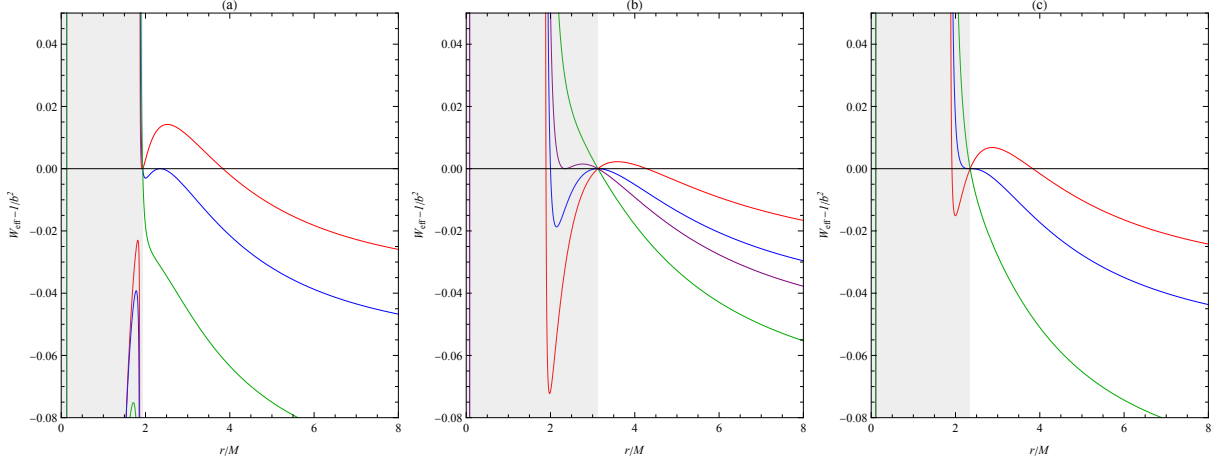


FIG. 4: Dimensionless effective potential $W_{\text{eff}}(r) - 1/b^2$ as a function of the radial distance r with the parameters b and λ in Fig. 3. (a): the parameter at points A1, A2, and A3; (b): the parameter at points B1, B2, B3, and D; (c): the parameter at points C1, C2, and C3. Note that the incident light ray has an effective zero energy from (16). The shaded area is inside the throat for reference.

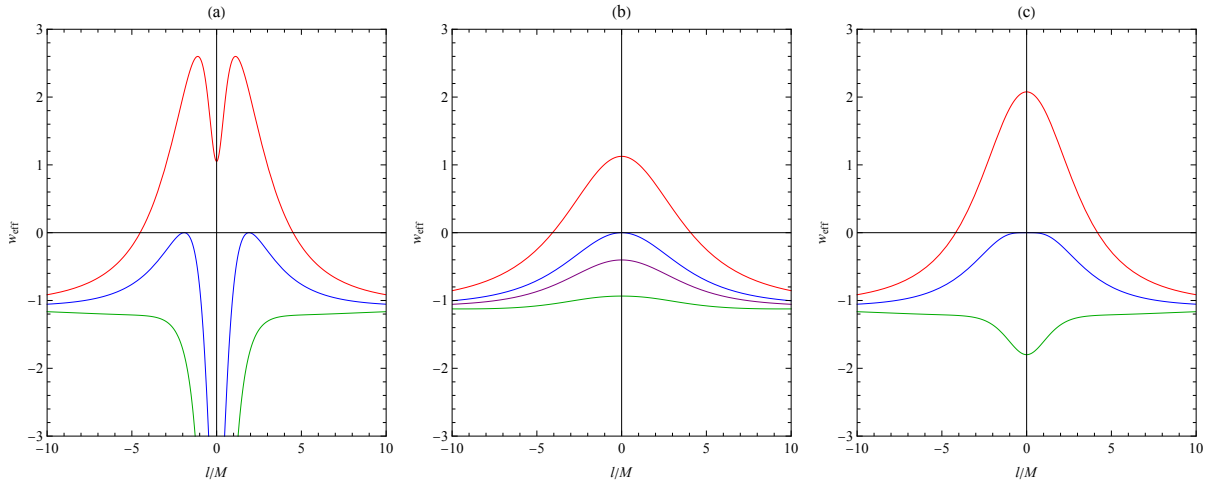


FIG. 5: Dimensionless effective potential $w_{\text{eff}}(l)$ as a function of the proper radial distance l with the parameters b and λ in Fig. 3. (a): the parameter at points A1, A2, and A3; (b): the parameter at points B1, B2, B3, and D; (c): the parameter at points C1, C2, and C3. Note that the incident light ray has an effective zero energy from (19).

A. The throat inside the light sphere: $r_{\text{th}} < r_4 = r_3 \equiv r_{sc}$

Let us now consider the cases of the unstable double root $r_3 = r_4$ of the radial potential $\tilde{R}(r)$ and also of $R(r)$ with a critical impact parameter $b(r_{sc}) \equiv b_{sc}$, forming the light sphere with the radius r_{sc} given by [21, 33],

$$r_{sc} = 2M \left\{ 1 + \cos \left[\frac{2}{3} \cos^{-1} \left(\frac{-sa}{M} \right) \right] \right\} \quad (27)$$

and

$$b_{sc} = b(r_{sc}) = -sa + 6M \cos \left[\frac{1}{3} \cos^{-1} \left(\frac{-sa}{M} \right) \right]. \quad (28)$$

The throat r_{th} is inside the double root. Therefore, we consider the roots following $r_4 = r_3 > r_{\text{th}}$ together with the deviation parameter $\lambda < \lambda_c$, where λ_c is determined by $r_{\text{th}}(\lambda_c) = r_{sc}$ for a specific spin a and is obtained as

$$\lambda_c = \sqrt{\frac{r_{sc}(r_{sc} - 2M) + a^2}{2Mr_{sc}}}. \quad (29)$$

We now start considering the impact parameter $b > b_c$ in the region of $r_4 > r_3 > r_{\text{th}}$ with a turning point $r_0 = r_4$. Therefore, light rays from spatial infinity will scatter off at r_4 and do not reach the throat. The deflection of the light rays is similar to that by a Kerr black hole but with the modification of the coefficients \bar{a} and \bar{b} due to the throat. Let us introduce the deflection angle

$$\hat{\alpha} + \pi = 2 \int_{r_0}^{\infty} \frac{br(r - 2M) + 2Msar}{\sqrt{(r - r_+)(r - r_-)(r - r_{\text{th}})(r - \tilde{r}_-)(r - r_1)(r - r_2)(r - r_3)(r - r_0)}} dr. \quad (30)$$

To do the integration, we change the variable to z

$$z \equiv 1 - \frac{r_0}{r} \quad (31)$$

and the integral can be rewritten as

$$\hat{\alpha} + \pi = 2r_0^2 \int_0^1 \frac{[r_0 + 2M(z - 1)]b - 2Msa(z - 1)}{\sqrt{\mathcal{B}(z, r_0)}} dz, \quad (32)$$

where the denominator

$$\begin{aligned} \mathcal{B}(z, r_0) &= r_0[r_0 + r_+(z - 1)][r_0 + r_-(z - 1)][r_0 + r_{\text{th}}(z - 1)][r_0 + \tilde{r}_-(z - 1)] \\ &\quad \times [r_0 + r_1(z - 1)][r_0 + r_2(z - 1)][r_0 + r_3(z - 1)]z \\ &= \sum_{n=1}^8 c_n(r_0)z^n \end{aligned} \quad (33)$$

and c_n 's are the series coefficients. In particular, the coefficient $c_1(r_0)$ is obtained as

$$c_1(r_0) = r_0(r_0 - r_+)(r_0 - r_-)(r_0 - r_{\text{th}})(r_0 - \tilde{r}_-)(r_0 - r_1)(r_0 - r_2)(r_0 - r_3), \quad (34)$$

which vanishes when $r_0 \rightarrow r_{sc} = r_3 = r_4$ while other coefficients remain nonzero. Now the deflection angle is a function of the closest approach distance r_0 given by (22) as

$$\hat{\alpha}(r_0) = I(r_0) - \pi, \quad I(r_0) = \int_0^1 f(z, r_0) dz \quad (35)$$

with the integrand function

$$f(z, r_0) = \frac{2r_0^2[r_0b + 2Mb(z-1) - 2Msa(z-1)]}{\sqrt{c_1z + c_2z^2 + c_3z^3 + c_4z^4 + c_5z^5 + c_6z^6 + c_7z^7 + c_8z^8}}. \quad (36)$$

In the limit $r_0 \rightarrow r_{sc}$ of the double root $r_3 = r_4$,

$$\begin{aligned} c_1(r_0) &\sim \mathcal{O}(r_0 - r_{sc}) \rightarrow 0, \\ c_i(r_0) &\sim \mathcal{O}(1), \end{aligned} \quad (37)$$

the integrand function $f(z, r_0) \rightarrow 1/z$ for small z , leading to the divergence. We then separate the divergence piece from the finite one, where the divergence can be extracted from the integral of the function

$$f_D(z, r_0) \equiv \frac{2r_0^2[r_0b + 2Mb(z-1) - 2Msa(z-1)]}{\sqrt{c_1z + c_2z^2}}, \quad (38)$$

such that the integration of

$$f_R(z, r_0) = f(z, r_0) - f_D(z, r_0) \quad (39)$$

over z is finite. First, we proceed by considering the divergent part,

$$\begin{aligned} I_D(r_0) &= \int_0^1 f_D(z, r_0) dz \\ &= - \frac{4Mr_0^2(sa-b)\sqrt{c_1+c_2}}{c_2} \\ &\quad + \frac{4r_0^2[Msa(c_1+2c_2) - Mbc_1 + b(r_0-2M)c_2]}{c_2^{3/2}} \log \left(\frac{\sqrt{c_1+c_2} - \sqrt{c_2}}{\sqrt{c_1}} \right). \end{aligned} \quad (40)$$

In the SDL, the expansions of the coefficient $c_1(r_0)$, and the impact parameter $b(r_0)$ in powers of small $r_0 - r_{sc}$ read

$$c_1(r_0) = c'_{1sc}(r_0 - r_{sc}) + \mathcal{O}(r_0 - r_{sc})^2 \quad (41)$$

and

$$b(r_0) = b_{sc} + \frac{1}{2!}b''_{sc}(r_0 - r_{sc})^2 + \mathcal{O}(r_0 - r_{sc})^3, \quad (42)$$

where $c'_{1sc} \equiv c'_1(r_{sc})$ and $b''_{sc} \equiv b''(r_{sc})$, and the prime means the derivative with respect to r_0 . Therefore, in the limit, the elements in the logarithm can be expanded as

$$\lim_{r_0 \rightarrow r_{sc}} \frac{\sqrt{c_1(r_0) + c_2(r_0)} - \sqrt{c_2(r_0)}}{\sqrt{c_1(r_0)}} = \frac{\sqrt{c'_{1sc}}}{2\sqrt{c_2(r_{sc})}}(r_0 - r_{sc})^{1/2}, \quad (43)$$

which are substituted into the divergent part I_D giving

$$I_D(r_0) \simeq - \frac{4Mr_{sc}^2(sa - b_{sc})}{\sqrt{c_{2sc}}} - \frac{2r_{sc}^2[2Msa + b_{sc}(r_{sc} - 2M)]}{\sqrt{c_{2sc}}} \log \left[\frac{c'_{1sc}}{4c_{2sc}}(r_0 - r_{sc}) \right]. \quad (44)$$

Or replacing r_0 by b through (42), the formula becomes

$$I_D(b) \simeq - \frac{r_{sc}^2[2Msa + b_{sc}(r_{sc} - 2M)]}{\sqrt{c_{2sc}}} \log \left(\frac{b}{b_{sc}} - 1 \right) - \frac{2r_{sc}^2[2Msa + b_{sc}(r_{sc} - 2M)]}{\sqrt{c_{2sc}}} \log \left(\frac{c'_{1sc}}{4c_{2sc}} \sqrt{\frac{2b_{sc}}{b''_{sc}}} \right) - \frac{4Mr_{sc}^2(sa - b_{sc})}{\sqrt{c_{2sc}}} \quad (45)$$

by the relation

$$\lim_{r_0 \rightarrow r_{sc}} (r_0 - r_{sc}) = \lim_{b \rightarrow b_{sc}} \sqrt{\frac{2}{b''_{sc}}}(b - b_{sc}). \quad (46)$$

Finally, the coefficients \bar{a} and b_D from the divergent part are

$$\bar{a} = \frac{r_{sc}^2[2Msa + b_{sc}(r_{sc} - 2M)]}{\sqrt{c_{2sc}}} \quad (47)$$

and

$$b_D = -2\bar{a} \log \left(\frac{c'_{1sc}}{4c_{2sc}} \sqrt{\frac{2b_{sc}}{b''_{sc}}} \right) - \frac{4Mr_{sc}^2(sa - b_{sc})}{\sqrt{c_{2sc}}}. \quad (48)$$

Here, we can verify the coefficients of the divergent term in another way. We first take the strong deflection limit such that $c_1(r_{sc}) = 0$. Then, we can expect the most of the contribution of the integral to come from the $z \rightarrow 0$ region. The natural lower limit can be set at $z \rightarrow c_1/c_2 = 2(r_0 - r_{sc})/r_{sc}$ when $c_1z \simeq c_2z^2$ in the function $f_D(z, r_0)$ for $r_0 \rightarrow r_{sc}$. So, the divergent part can be found to be

$$\begin{aligned} I_D(r_0) &\simeq \int_0^1 \lim_{z \rightarrow 0} f_D(z, r_{sc}) dz \\ &= \frac{2r_{sc}^2[r_{sc}b_{sc} - 2Mb_{sc} + 2Msa]}{\sqrt{c_{2sc}}} \int_{z \rightarrow \frac{2}{r_{sc}}(r_0 - r_{sc})}^1 \frac{1}{z} dz + \text{finite part} \\ &\sim - \frac{2r_{sc}^2[r_{sc}b_{sc} - 2Mb_{sc} + 2Msa]}{\sqrt{c_{2sc}}} \log(r_0 - r_{sc}) + \text{finite part}. \end{aligned} \quad (49)$$

Or we can also rewrite I_D as a function of the impact parameter through (46),

$$I_D(b) \sim -\frac{r_{sc}^2 [2Msa + b_{sc}(r_{sc} - 2M)]}{\sqrt{c_{2sc}}} \log \left(\frac{b}{b_{sc}} - 1 \right). \quad (50)$$

Moreover, we would like to ask whether the coefficient \bar{a} due to a Kerr-like wormhole can be reduced to the Kerr black hole \bar{a} in [22, 23]. By turning off the deviation parameter λ , the throat r_{th} reduces to r_+ and $\tilde{r}_- = r_-$. The coefficient c_{2sc} in \bar{a} becomes

$$c_{2sc} = r_{sc}^2 (r_{sc} - r_+)^2 (r_{sc} - r_-)^2 (r_{sc} - r_1)(r_{sc} - r_2), \quad (51)$$

where the roots $r_1 = -2r_{sc}$ due to $r_2 = 0$ and the property $r_1 + r_2 + r_3 + r_4 = 0$ in [32]. Then, together with the condition of the light sphere [33]

$$r_{sc}^2 - 3Mr_{sc} + 2sa\sqrt{Mr_{sc}} = 0, \quad (52)$$

the coefficient becomes

$$\bar{a}|_{\lambda=0} = \frac{2Mr_{sc}}{(r_{sc} - M)\sqrt{3Mr_{sc}}}, \quad (53)$$

which is the coefficient of the divergent term from a Kerr black hole [22].

The subleading order term is from the integration of $f_R(z, r_{sc})$ in (39) denoted by b_R ,

$$b_R = I_R(r_{sc}) = \int_0^1 f_R(z, r_{sc}) dz, \quad (54)$$

which is a constant in the deflection angle to be computed numerically. Thus, the coefficient \bar{b} can be computed from the sum of b_D and b_R

$$\bar{b} = -\pi + b_D + b_R. \quad (55)$$

We now consider an alternative approach from $b < b_{sc}$ in the region of $r_4 = r_3^*$ of a pair of complex conjugates in Fig. 3. In this case, there is no turning point outside the throat with the impact parameter b so that light rays pass through the throat. In this case, the deflection angle (30) in terms of z can be defined as

$$z = 1 - \frac{r_{sc}}{r} \quad (56)$$

with $r_3 = r_4 = r_{sc}$, and becomes

$$\hat{\alpha} + \pi = 2r_{sc}^2 \int_{1-\frac{r_{sc}}{r_{th}}}^1 \frac{[r_{sc} + 2M(z-1)]b - 2Msa(z-1)}{\sqrt{\mathcal{B}(z, b)}} dz, \quad (57)$$

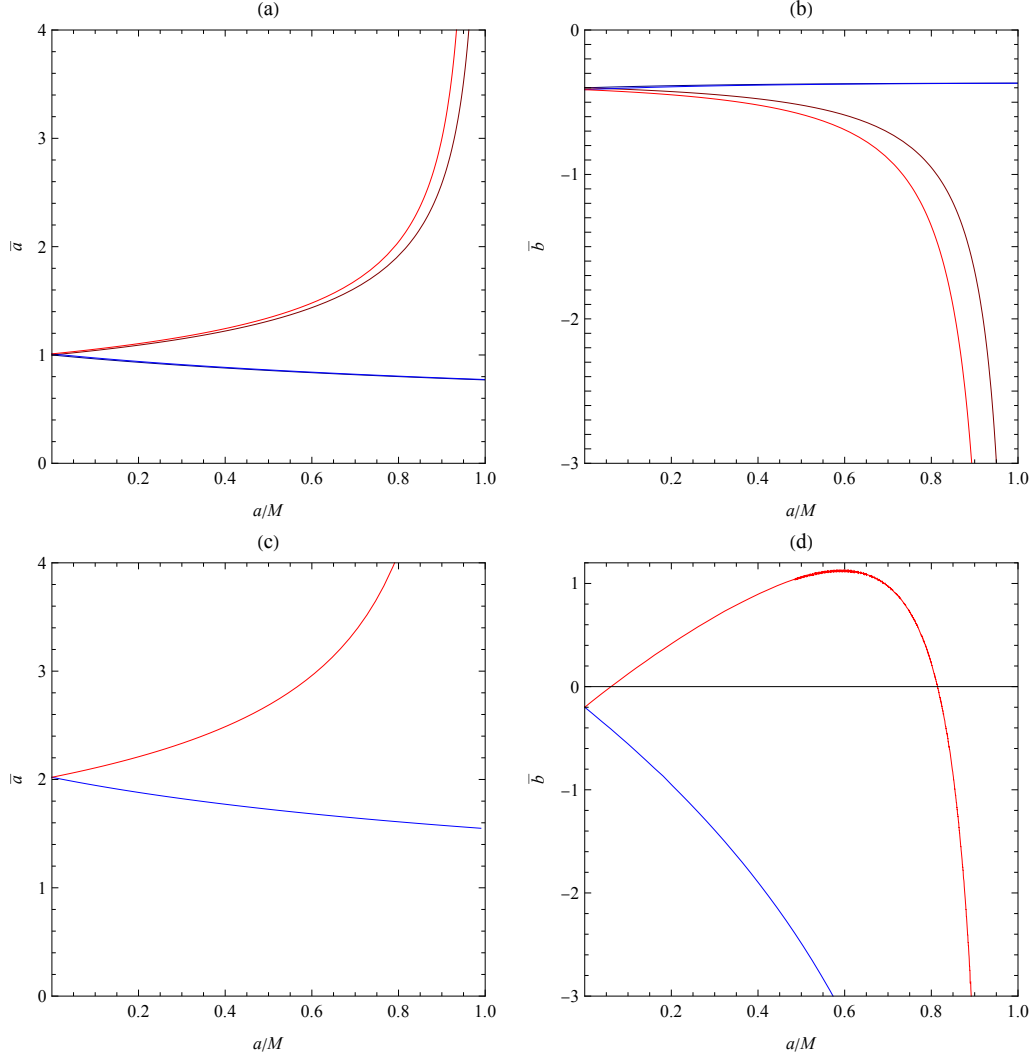


FIG. 6: (a): the coefficients \bar{a} as the functions of the spin a with (47) from $b > b_{sc}$; (b): the coefficients \bar{b} as the functions of the spin a with (55) from $b > b_{sc}$, for direct orbit in the red (deep red) line and retrograde orbit in the blue (deep blue) line for $\lambda = 0$ ($\lambda = 0.1$); (c): the coefficients \bar{a} as the functions of the spin a with (64) from $b < b_{sc}$; (d): the coefficients \bar{b} as the functions of the spin a with (55) from $b < b_{sc}$ for direct orbit in the red line and retrograde orbit in the blue line for $\lambda = 0.1$. Note that, the SDL deflection angle with $b < b_{sc}$ cannot be reduced to the Kerr black hole case since the light ray cannot travel through a black hole.

where the denominator

$$\begin{aligned} \mathcal{B}(z, b) &= [r_{sc} + r_+(z-1)][r_{sc} + r_-(z-1)][r_{sc} + r_{th}(z-1)][r_{sc} + \tilde{r}_-(z-1)] \\ &\quad \times [r_{sc} + r_1(z-1)][r_{sc} + r_2(z-1)][r_{sc} + r_3(z-1)][r_{sc} + r_4(z-1)] \\ &= \sum_{n=0}^8 c_n(b) z^n \end{aligned} \quad (58)$$

with the coefficient

$$c_0(b) = (r_{sc} - r_+)(r_{sc} - r_-)(r_{sc} - r_{th})(r_{sc} - \tilde{r}_-)(r_{sc} - r_1)(r_{sc} - r_2)(r_{sc} - r_3)(r_{sc} - r_4) \quad (59)$$

and the roots r_i 's are functions of b . As $b \rightarrow b_{sc}$, the two roots $r_3, r_4 \rightarrow r_{sc}$. The integrand function, giving the divergence of the deflection angle in the limit of the double root, is then given by

$$f_D(z, b) \equiv \frac{2r_{sc}^2[r_{sc}b + 2Mb(z-1) - 2Msa(z-1)]}{\sqrt{c_0 + c_1z + c_2z^2}}. \quad (60)$$

After the integration over z , $I_D(b)$ is obtained as

$$\begin{aligned} I_D(b) &= -\frac{4r_{sc}^2M(sa-b)(1-\frac{r_{sc}-r_{th}}{r_{th}})}{\sqrt{c_2(b)}} + \frac{2r_{sc}^2[2Msa + b(r_{sc} - 2M)]}{\sqrt{c_2(b)}} \log \left(\frac{\sqrt{c_0 + c_1 + c_2} - \sqrt{c_0} + \sqrt{c_2}}{\sqrt{c_0 + c_1 + c_2} - \sqrt{c_0} - \sqrt{c_2}} \right) \\ &\quad - \frac{2r_{sc}^2[2Msa + b(r_{sc} - 2M)]}{\sqrt{c_2(b)}} \log \left[\frac{\sqrt{r_{th}(c_0r_{th} - c_1r_{sc} + c_1r_{th}) + c_2(r_{sc} - r_{th})^2} - \sqrt{c_0}r_{th} - \sqrt{c_2}(r_{sc} - r_{th})}{\sqrt{r_{th}(c_0r_{th} - c_1r_{sc} + c_1r_{th}) + c_2(r_{sc} - r_{th})^2} - \sqrt{c_0}r_{th} + \sqrt{c_2}(r_{sc} - r_{th})} \right]. \end{aligned} \quad (61)$$

Hence, we expand the coefficients $c_0(b)$ and $c_1(b)$ around b_{sc} ,

$$\begin{aligned} c_0(b) &= c'_0(b_{sc})(b - b_{sc}) + \mathcal{O}(b - b_{sc})^2, \\ c_1(b) &= c'_1(b_{sc})(b - b_{sc}) + \mathcal{O}(b - b_{sc})^2, \end{aligned} \quad (62)$$

where the prime means the derivative with respect to b and $c'_0(b_{sc}), c'_1(b_{sc}) < 0$, while other $c_n(b_{sc})$ are nonzero. So, the integral $I_D(b)$ becomes

$$\begin{aligned} I_D(b) &\simeq -\frac{2r_{sc}^2[2Msa + b_{sc}(r_{sc} - 2M)]}{\sqrt{c_2(b_{sc})}} \log \left(\frac{b_{sc}}{b} - 1 \right) \\ &\quad - \frac{2r_{sc}^2[2Msa + b_{sc}(r_{sc} - 2M)]}{\sqrt{c_2(b_{sc})}} \log \left(\frac{-b_{sc}c'_0(b_{sc})}{4c_2(b_{sc})} \frac{r_{th}}{r_{sc} - r_{th}} \right) - \frac{4Mr_{sc}^2(sa - b_{sc})(2r_{th} - r_{sc})}{\sqrt{c_2(b_{sc})}r_{th}}, \end{aligned} \quad (63)$$

and the coefficients \bar{a} and b_D are obtained as

$$\bar{a} = \frac{2r_{sc}^2[2Msa + b_{sc}(r_{sc} - 2M)]}{\sqrt{c_2(b_{sc})}} \quad (64)$$

and

$$b_D = -\bar{a} \log \left(\frac{-b_{sc} c'_0(b_{sc})}{4c_2(b_{sc})} \frac{r_{th}}{r_{sc} - r_{th}} \right) - \frac{4Mr_{sc}^2(sa - b_{sc})(2r_{th} - r_{sc})}{\sqrt{c_2(b_{sc})}r_{th}}. \quad (65)$$

Then, the value of b_R can be computed from the integral of $f_R(z, b_{sc})$ to be done numerically. Thus, the coefficient \bar{b} can be calculated from the sum of b_D and b_R in (55).

Notice that in general \bar{a} and \bar{b} in (64) and (65) from $b < b_{sc}$ are different from those in (47) and (48) from $b > b_{sc}$. A factor 2 difference in \bar{a} between (64) and (47) can be attributed to the fact that from $b > b_{sc}$ toward $b \rightarrow b_{sc}$, the light ray will hit the turning point $r_0 = r_4$ and deflect to another direction as seen in the graphs in Fig. 5. However, from $b < b_{sc}$, the light ray will pass through the throat to another spacetime also seen in Fig. 5. When $b \rightarrow b_{sc}$ with two developed unstable maxima associated with each spacetime, the light ray may travel between them, giving the extra the factor 2 in \bar{a} compared to the case of $b > b_{sc}$. The coefficient \bar{b} is different between both cases. The coefficients \bar{a} and \bar{b} for the direct and retrograde orbits from both $b > b_{sc}$ and $b < b_{sc}$ as approaching to the double root are plotted with a finite λ as compared with the Kerr case with $\lambda = 0$ in Fig. 6, where \bar{a} and $|\bar{b}|$ increase in λ . The corresponding deflection angle in the SDL is shown in Fig. 7.

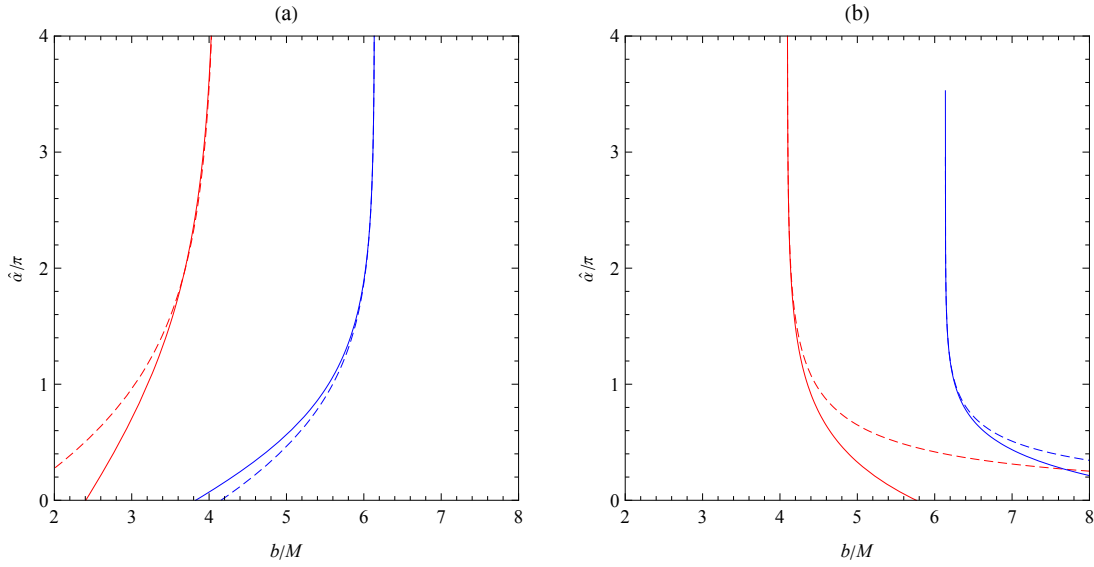


FIG. 7: The SDL deflection angle $\hat{\alpha}(b)$ from $b < b_{sc}$ in (a) with (25), (64), and (55); from $b > b_{sc}$ in (b) with (23), (47), and (55), for the direct and retrograde orbits with $a = 0.5$ and $\lambda = 0.3$. The numerical results are displayed in the dashed lines for comparison.

B. The throat as a light sphere: $r_{\text{th}} = r_4$

Let us now consider the cases when the throat together with r_4 becomes an unstable double root $r_{\text{th}} = r_4$ with the parameters along the corresponding line in Fig. 3 and the deviation parameter $\lambda > \lambda_c$, where $r_{\text{th}}(\lambda_c) = r_{sc}$ resulting from the requirements of $\tilde{R}(r)|_{r=r_{\text{th}}} = \tilde{R}'(r)|_{r=r_{\text{th}}} = 0$ and $\tilde{R}''(r)|_{r=r_{\text{th}}} > 0$. They allow light rays to have rather unique unstable circular orbits with radius determined by the throat r_{th} , forming a light sphere [27]. The root relationship is as follows: $r_{\text{th}} = r_4 > r_3$. The limit of $r_{\text{th}} = r_4$ can be approached either from $b > b_{\text{th}}$ or from $b < b_{\text{th}}$.

In the former case, we start from b in the region of $r_4 > r_{\text{th}}$ and $\lambda > \lambda_c$. So, the turning point is set at $r_0 = r_4$ with the impact parameter $b(r_0)$. We introduce the variable z as usual and rewrite the integration in (30) as in (32) with the same $\mathcal{B}(z, r_0)$. Then, the integral of the divergent part gives the same result of (40). In the limit $r_0 \rightarrow r_{\text{th}}$,

$$\begin{aligned} c_1(r_0) &\sim \mathcal{O}(r_0 - r_{\text{th}}) \rightarrow 0, \\ c_i(r_0) &\sim \mathcal{O}(1). \end{aligned} \tag{66}$$

We expand the coefficient $c_1(r_0)$ and the impact parameter $b(r_0)$ in terms of $r_0 - r_{\text{th}}$,

$$c_1(r_0) = c'_{1\text{th}}(r_0 - r_{\text{th}}) + \mathcal{O}(r_0 - r_{\text{th}})^2, \tag{67}$$

and

$$b(r_0) = b_{\text{th}} + b'_{\text{th}}(r_0 - r_{\text{th}}) + \mathcal{O}(r_0 - r_{\text{th}})^2, \tag{68}$$

where $c'_{1\text{th}} \equiv c'_1(r_{\text{th}})$ and the surviving $b'_{\text{th}} \equiv b'(r_{\text{th}})$. So, when we replace r_0 by $b(r_0)$, the divergent part becomes

$$\begin{aligned} I_D(b) &\simeq - \frac{2r_{\text{th}}^2 [2Msa + b_{\text{th}}(r_{\text{th}} - 2M)]}{\sqrt{c_{2\text{th}}}} \log \left(\frac{b}{b_{\text{th}}} - 1 \right) \\ &\quad - \frac{2r_{\text{th}}^2 [2Msa + b_{\text{th}}(r_{\text{th}} - 2M)]}{\sqrt{c_{2\text{th}}}} \log \left(\frac{c'_{1\text{th}} b_{\text{th}}}{4c_{2\text{th}} b'_{\text{th}}} \right) - \frac{4Mr_{\text{th}}^2 (sa - b_{\text{th}})}{\sqrt{c_{2\text{th}}}} \end{aligned} \tag{69}$$

given by the relation of (68)

$$\lim_{r_0 \rightarrow r_{\text{th}}} (r_0 - r_{\text{th}}) = \lim_{b \rightarrow b_{\text{th}}} \frac{1}{b'_{\text{th}}} (b - b_{\text{th}}). \tag{70}$$

Finally, the coefficients \bar{a} and b_D for the divergent part are

$$\bar{a} = \frac{2r_{\text{th}}^2 [2Msa + b_{\text{th}}(r_{\text{th}} - 2M)]}{\sqrt{c_{2\text{th}}}} \tag{71}$$

and

$$b_D = -\bar{a} \log \left(\frac{c'_{1\text{th}} b_{\text{th}}}{4c_{2\text{th}} b'_{\text{th}}} \right) - \frac{4Mr_{\text{th}}^2(sa - b_{\text{th}})}{\sqrt{c_{2\text{th}}}}. \quad (72)$$

By replacing r_{sc} with r_{th} , the value of b_R obtained from the integral of the function $f_R(z, r_{\text{th}})$ can be calculated by (54). Thus, the coefficient \bar{b} can be computed from the sum of b_D and b_R in (55).

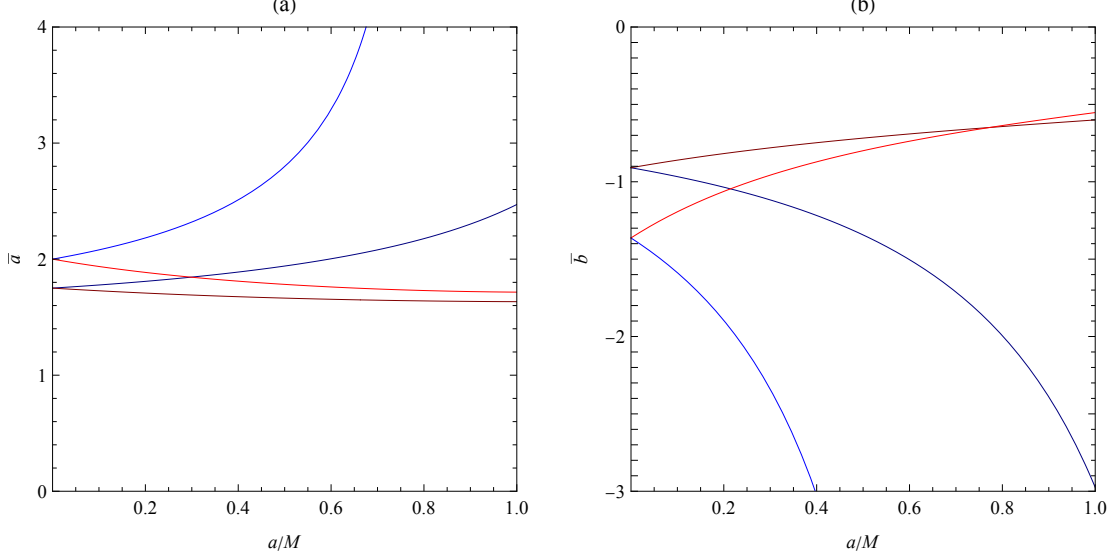


FIG. 8: (a): the coefficients \bar{a} as the functions of the spin a with (71) from both $b > b_{\text{th}}$ or $b < b_{\text{th}}$; (b): the coefficients \bar{b} as the functions of the spin a with (72) from both $b > b_{\text{th}}$ or $b < b_{\text{th}}$, for direct orbit in the red (deep red) line and retrograde orbit in the blue (deep blue) line for $\lambda = 1.0$ ($\lambda = 1.2$).

For the unstable double root $r_{\text{th}} = r_4$ approaching from $b < b_{\text{th}}$, we start with the impact parameter b in the region of $r_{\text{th}} > r_4 > r_3$ and $\lambda > \lambda_c$ in Fig. 3. Then, the deflection angle (30) in terms of z defined to be

$$z = 1 - \frac{r_{\text{th}}}{r} \quad (73)$$

becomes

$$\hat{\alpha} + \pi = 2r_{\text{th}}^2 \int_0^1 \frac{[r_{\text{th}} + 2M(z-1)]b - 2Msa(z-1)}{\sqrt{\mathcal{B}(z, b)}} dz, \quad (74)$$

where the denominator

$$\begin{aligned} \mathcal{B}(z, b) &= r_{\text{th}}[r_{\text{th}} + r_+(z-1)][r_{\text{th}} + r_-(z-1)][r_{\text{th}} + \tilde{r}_-(z-1)] \\ &\quad \times [r_{\text{th}} + r_1(z-1)][r_{\text{th}} + r_2(z-1)][r_{\text{th}} + r_3(z-1)][r_{\text{th}} + r_4(z-1)]z \\ &= \sum_{n=1}^8 c_n(b)z^n \end{aligned} \quad (75)$$

with the coefficient

$$c_1(b) = r_{\text{th}}(r_{\text{th}} - r_+)(r_{\text{th}} - r_-)(r_{\text{th}} - \tilde{r}_-)(r_{\text{th}} - r_1)(r_{\text{th}} - r_2)(r_{\text{th}} - r_3)(r_{\text{th}} - r_4) \quad (76)$$

and the roots r_i 's are functions of b . Moreover, $r_4 \rightarrow r_{\text{th}}$ as $b \rightarrow b_{\text{th}}$.

Then, the integrand function potentially leads to the divergence of the deflection angle as approaching the double root is given by

$$f_D(z, b) \equiv \frac{2r_{\text{th}}^2[r_{\text{th}}b + 2Mb(z-1) - 2Msa(z-1)]}{\sqrt{c_1z + c_2z^2}}, \quad (77)$$

and after integration over z ,

$$I_D(b) = -\frac{4r_{\text{th}}^2M(sa-b)}{\sqrt{c_2(b)}} - \frac{4r_{\text{th}}^2[2Msa + b(r_{\text{th}} - 2M)]}{\sqrt{c_2(b)}} \log \left(\frac{\sqrt{c_1(b) + c_2(b)} - \sqrt{c_2(b)}}{\sqrt{c_1(b)}} \right). \quad (78)$$

Hence, we expand the coefficient $c_1(b)$ around b_{th} ,

$$c_1(b) = c'_1(b_{\text{th}})(b - b_{\text{th}}) + \mathcal{O}(b - b_{\text{th}})^2, \quad (79)$$

where $c'_1(b_{\text{th}}) < 0$, while other $c_n(b_{\text{th}})$ are nonzero and therefore

$$\lim_{b \rightarrow b_{\text{th}}} \frac{\sqrt{c_1(b) + c_2(b)} - \sqrt{c_2(b)}}{\sqrt{c_1(b)}} = \frac{\sqrt{-c'_1(b_{\text{th}})b}}{2\sqrt{c_2(b_{\text{th}})}} \left(\frac{b_{\text{th}}}{b} - 1 \right)^{1/2} \quad (80)$$

for $b \lesssim b_{\text{th}}$. So, $I_D(b)$ becomes

$$\begin{aligned} I_D(b) &\simeq -\frac{2r_{\text{th}}^2[2Msa + b_{\text{th}}(r_{\text{th}} - 2M)]}{\sqrt{c_2(b_{\text{th}})}} \log \left(\frac{b_{\text{th}}}{b} - 1 \right) \\ &\quad - \frac{4r_{\text{th}}^2[2Msa + b_{\text{th}}(r_{\text{th}} - 2M)]}{\sqrt{c_2(b_{\text{th}})}} \log \left(\frac{\sqrt{-b_{\text{th}}c'_1(b_{\text{th}})}}{2\sqrt{c_2(b_{\text{th}})}} \right) - \frac{4Mr_{\text{th}}^2(sa - b_{\text{th}})}{\sqrt{c_2(b_{\text{th}})}}, \end{aligned} \quad (81)$$

and the coefficients \bar{a} , b_D are written as

$$\bar{a} = \frac{2r_{\text{th}}^2[2Msa + b_{\text{th}}(r_{\text{th}} - 2M)]}{\sqrt{c_2(b_{\text{th}})}} \quad (82)$$

and

$$b_D = -\bar{a} \log \left(\frac{-b_{\text{th}} c_1'(b_{\text{th}})}{4c_2(b_{\text{th}})} \right) - \frac{4Mr_{\text{th}}^2(sa - b_{\text{th}})}{\sqrt{c_2(b_{\text{th}})}}. \quad (83)$$

Then, the value of b_R can be estimated from the integral of $f_R(z, b_{\text{th}})$ through (54). Thus, the coefficient \bar{b} can be calculated from the sum of b_D and b_R in (55). Then, the SDL deflection angle can be summarized as

$$\hat{\alpha}(b) \approx -\bar{a} \log \left(\frac{b_c}{b} - 1 \right) + \bar{b} + O(b_c - b) \log(b_c - b). \quad (84)$$

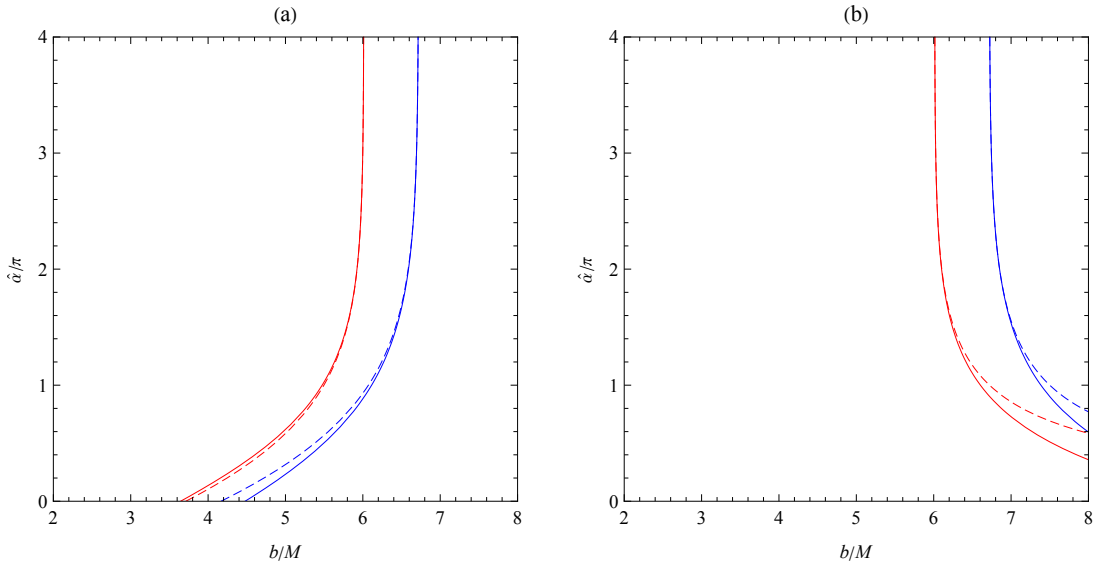


FIG. 9: The SDL deflection angle $\hat{\alpha}(b)$ from $b < b_{\text{th}}$ in (a) with (84); from $b > b_{\text{th}}$ in (b) with (23), (71), and (72), for the direct and retrograde orbits with $a = 0.5$ and $\lambda = 1.2$. The numerical results are displayed in the dashed lines for comparison.

It is worth mentioning that \bar{a} and b_D from both $b > b_{\text{th}}$ and $b < b_{\text{th}}$ in (71), (72), (82), (83) together with the respective b_R are the same. It is anticipated from the graphs of Fig. 5 that the approaches from both sides merge to the case that the throat resides on the light sphere. Fig. 8 shows that \bar{a} and \bar{b} from both $b > b_{\text{th}}$ and $b < b_{\text{th}}$ as approaching to the double root $r_4 = r_{\text{th}}$, where \bar{a} and $|\bar{b}|$ decrease in λ . The deflection angle in the SDL is plotted in Fig. 9.

C. The throat as a triple root: $r_{\text{th}} = r_4 = r_3 \equiv r_{sc}$

Another unique feature of the wormholes is that there exists a triple root of the radial potential $\tilde{R}(r)$ on the throat, namely $r_{\text{th}} = r_4 = r_3 \equiv r_{sc}$ when $r_{\text{th}} = r_{sc}$ leads to $\lambda = \lambda_c$ in (29) with the parameters shown in Fig. 3. They are determined by $r_{sc} = r_{\text{th}}$, where r_{sc} obeys $R(r)|_{r=r_{sc}} = R'(r)|_{r=r_{sc}} = 0$. We consider the impact parameter b lying on the region of $r_4 > r_{\text{th}}$ along with the line with a specific value of λ_c . Then, the turning point is set at $r_0 = r_4$. In terms of the variable z in (31), the deflection angle in (30) then becomes (32) with the coefficients in (33). The difference is that when r_0 gets close to r_{sc} , or $b \rightarrow b_{sc}$, the turning point $r_0 = r_4$ will simultaneously approach to r_3 and r_{th} . Therefore, in this triple root case,

$$\begin{aligned} c_1(r_0) &\sim \mathcal{O}(r_0 - r_{sc})^2 \rightarrow 0, \\ c_2(r_0) &\sim \mathcal{O}(r_0 - r_{sc}) \rightarrow 0, \end{aligned} \quad (85)$$

whereas other $c_n(r_{sc})$ are nonzero.

With that in mind, we introduce a new function, which gives the divergent part of the deflection angle after the integration over z as r_0 approach to the triple root, to be

$$f_D(z, r_0) \equiv \frac{2r_0^2[r_0b + 2Mb(z-1) - 2Msa(z-1)]}{\sqrt{c_1z + c_2z^2 + c_3z^3}}, \quad (86)$$

and then the integration of the remaining part $f_R(z, r_0) = f(z, r_0) - f_D(z, r_0)$ is finite. Now we take the limit of $r_0 = r_{sc}$, where $c_1(r_{sc})$ and $c_2(r_{sc})$ vanish. Then, the most significant contribution of the integral as $r_0 \rightarrow r_{sc}$ comes from the $z \rightarrow 0$ region, where a natural lower limit can be set when $c_1z \simeq c_2z^2 \simeq c_3z^3$ by $z \rightarrow \sqrt{c_1/c_3}$ or c_2/c_3 , and $c_1/c_2 = (r_0 - r_{sc})/r_{sc}$. So, we can find the divergent part as follows

$$\begin{aligned} I_D(r_0) &\simeq \int_0^1 \lim_{z \rightarrow 0} f_D(z, r_{sc}) dz \\ &= \frac{2r_{sc}^2[r_{sc}b_{sc} - 2Mb_{sc} + 2Msa]}{\sqrt{c_{3sc}}} \int_0^1 \frac{1}{z^{3/2}} dz + \mathcal{O}(z^{1/2}) \\ &\sim \frac{4r_{sc}^2[r_{sc}b_{sc} - 2Mb_{sc} + 2Msa]}{\sqrt{c_{3sc}}} z^{-1/2} \Big|_{z \rightarrow \frac{1}{r_{sc}}(r_0 - r_{sc})} + \text{finite part.} \end{aligned} \quad (87)$$

In terms of the impact parameter given by (42), the lower limit can be set at

$$z \rightarrow \sqrt{\frac{2}{b_{sc}'' r_{sc}^2}} (b - b_{sc})^{1/2}. \quad (88)$$

The divergent part $I_D(b)$ can be approximated by

$$I_D(b) \simeq \frac{4r_{sc}^{5/2}[2Msa + b_{sc}(r_{sc} - 2M)]}{\sqrt{c_{3sc}}} \left(\frac{b''_{sc}}{2b_{sc}}\right)^{1/4} \left(\frac{b}{b_{sc}} - 1\right)^{-1/4} + \text{finite part.} \quad (89)$$

Finally, the divergent part of the deflection angle has a power-law dependence of $b/b_{sc} - 1$ as $r_0 \rightarrow r_{sc}$, which shows non-logarithmic divergence. And the coefficients are shown as

$$\bar{a} = \frac{4r_{sc}^{5/2}[2Msa + b_{sc}(r_{sc} - 2M)]}{\sqrt{c_{3sc}}} \left(\frac{b''_{sc}}{2b_{sc}}\right)^{1/4} \quad (90)$$

and

$$b_D = -\frac{4r_{sc}^2[2Msa + b_{sc}(r_{sc} - 2M)]}{\sqrt{r_{sc}/M}\sqrt{c_{3sc}}}, \quad (91)$$

where the finite part b_D is obtained from the upper limit of the integral. In the non-rotating limit, $a \rightarrow 0$, the coefficient \bar{a} is reduced to a number 2.5558 and $b_D = -4/3$ in Schwarzschild-like wormholes [25].

Moreover, the subleading term for the triple root cases is from the integration of $f_R(z, r_{sc})$, giving b_R from (54). Again, the coefficient \bar{b} can be calculated from the sum of b_D and b_R in (55). To summarize, in the cases of triple root, the deflection angle in the SDL is written in the form

$$\hat{\alpha}(b) = \bar{a} \left(\frac{b}{b_{sc}} - 1\right)^{-1/4} + \bar{b} \quad (92)$$

with coefficients $\bar{a} > 0$ and \bar{b} . The divergence of the deflection angle as r_0 approaches the triple root is stronger than the double roots.

One can approach to the triple root from $b < b_{sc}$, where there is no turning point and the throat is exactly on the light sphere seen in Figs. 3 and 5. In terms of z in (73), the divergent part of the integral is given by

$$f_D(z, b) \equiv \frac{2r_{sc}^2[r_{sc}b + 2Mb(z-1) - 2Msa(z-1)]}{\sqrt{c_1z + c_2z^2 + c_3z^3}}, \quad (93)$$

where the coefficients

$$\begin{aligned} c_1(b) &\sim \mathcal{O}(b_{sc} - b) \rightarrow 0, \\ c_2(b) &\sim \mathcal{O}(b_{sc} - b) \rightarrow 0. \end{aligned} \quad (94)$$

We then obtain the integration of the divergent part by setting $b = b_{sc}$ giving $c_1(b_{sc}) =$

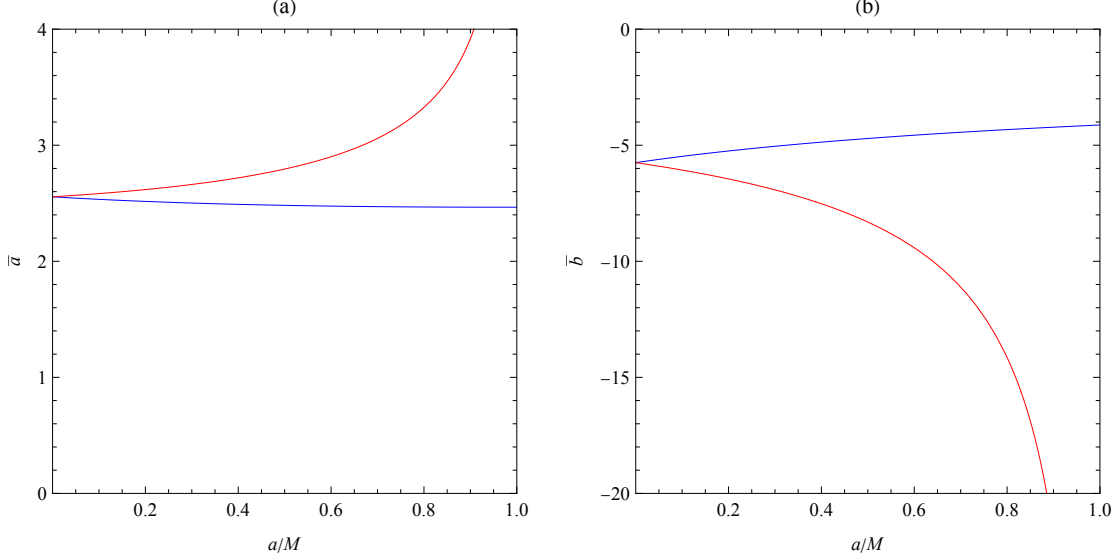


FIG. 10: (a) the coefficients \bar{a} as the functions of the spin a with (90) from both $b > b_{sc}$ or $b < b_{sc}$; (b) the coefficients \bar{b} as the functions of the spin a with (55) from both $b > b_{sc}$ or $b < b_{sc}$, for direct orbit in the red line and retrograde orbit in the blue line for $\lambda = \lambda_c(r_{sc})$.

$c_2(b_{sc}) = 0$ in the integrand

$$\begin{aligned}
I_D(b) &\simeq \int_0^1 \lim_{z \rightarrow 0} f_D(z, b_{sc}) dz \\
&= \frac{2r_{sc}^2[r_{sc}b_{sc} - 2Mb_{sc} + 2Msa]}{\sqrt{c_3(b_{sc})}} \int_0^1 \frac{1}{z^{3/2}} dz + \mathcal{O}(z^{1/2}) \\
&\sim \frac{4r_{sc}^2[r_{sc}b_{sc} - 2Mb_{sc} + 2Msa]}{\sqrt{c_3(b_{sc})}} z^{-1/2} \Big|_{z \rightarrow \sqrt{\frac{c_1}{c_3}}} + \text{finite part},
\end{aligned} \tag{95}$$

where the lower limit can be set at

$$z \rightarrow \sqrt{\frac{c_1}{c_3}} = \sqrt{\frac{-c'_1(b_{sc})}{c_3(b_{sc})}} (b_{sc} - b)^{1/2}, \tag{96}$$

which is the same as in (88) with the different expression. Therefore, the divergent part should be

$$I_D(b) \simeq \frac{4r_{sc}^2[2Msa + b_{sc}(r_{sc} - 2M)]}{\sqrt{c_3(b_{sc})}} \left(\frac{c_3(b_{sc})}{-b_{sc}c'_1(b_{sc})} \right)^{1/4} \left(\frac{b_{sc}}{b} - 1 \right)^{-1/4} + \text{finite part}, \tag{97}$$

with the coefficients shown as

$$\bar{a} = \frac{4r_{sc}^2[2Msa + b_{sc}(r_{sc} - 2M)]}{\sqrt{c_3(r_{sc})}} \left(\frac{c_3(b_{sc})}{-b_{sc}c'_1(b_{sc})} \right)^{1/4} \tag{98}$$

and

$$b_D = -\frac{4r_{sc}^2[2Msa + b_{sc}(r_{sc} - 2M)]}{\sqrt{r_{sc}/M}\sqrt{c_3(b_{sc})}}. \quad (99)$$

Again, the finite part b_D can be obtained from the upper limit of the integral. To summarize, in the cases of the triple root, the deflection angle in the SDL is written in the form

$$\hat{\alpha}(b) = \bar{a} \left(\frac{b_{sc}}{b} - 1 \right)^{-1/4} + \bar{b}. \quad (100)$$

Based on the effective potential $w_{\text{eff}}(l)$ in Fig. 5 with a similar behavior in the case of $\lambda > \lambda_c$, we expect that \bar{a} and \bar{b} from $b < b_{sc}$ are the same as from $b > b_{sc}$. Fig. 10 shows \bar{a} and \bar{b} with the deflection angle of the power-law divergence on the triple roots from both $b < b_{sc}$ and $b > b_{sc}$ in Fig. 11.

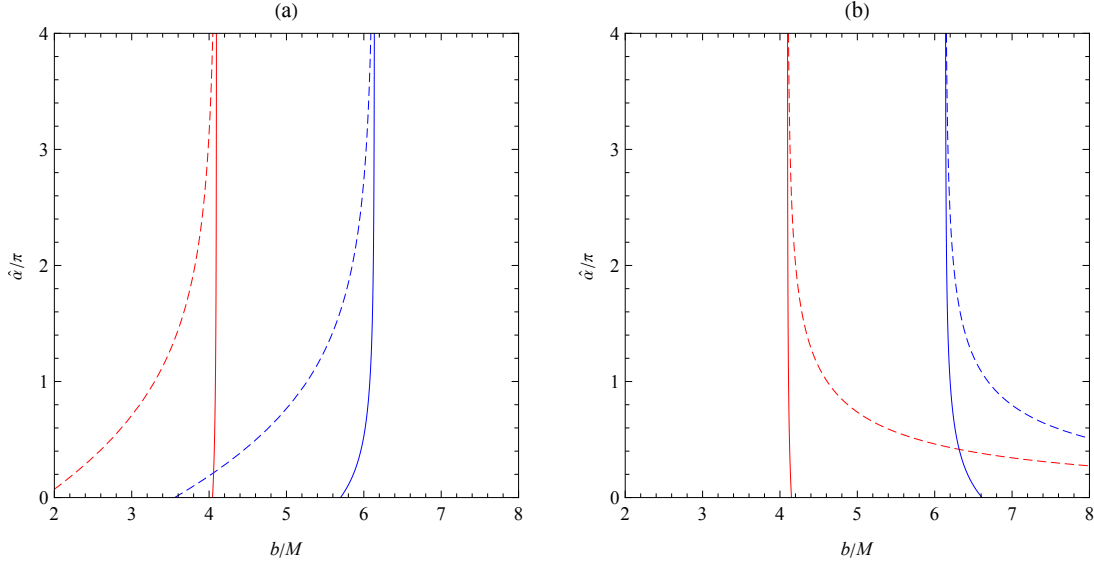


FIG. 11: The SDL deflection angle $\hat{\alpha}(b)$ from $b < b_{sc}$ in (a) with (100); from $b > b_{sc}$ in (b) with (92), for the direct and retrograde orbits with $a = 0.5$ and $\lambda = \lambda_c(\pm a)$. The numerical solutions are shown in the dashed lines for comparison.

D. The throat outside the double root: $r_{\text{th}} > r_4 = r_3 \equiv r_{sc}$

For completeness, let us also consider the case $r_4 = r_3 < r_{\text{th}}$ with the parameters along the line shown in Fig. 3, although the light rays will not reach the double root and will only

see the throat. We start by choosing the impact parameter b in the region of $r_3 < r_4 < r_{\text{th}}$. In particular, when $r_{\text{th}} > r_4$, this is a unique case for wormholes, where the light rays can pass through the throat to another spacetime without seeing the roots of r_3 and r_4 , which can be visualized in Fig. 6 of [30]. We introduce the variable

$$u \equiv \frac{r_{\text{th}}}{r}, \quad (101)$$

and then the integration in (30) can be rewritten as

$$\hat{\alpha} + \pi = 2 \int_0^1 f_T(u, b) du, \quad (102)$$

where the integrated function is

$$f_T(u, b) = \frac{\frac{2Ms a}{r_{\text{th}}^2} u + \frac{b}{r_{\text{th}}} \left(1 - \frac{2M}{r_{\text{th}}} u\right)}{\sqrt{\left(1 - \frac{2M}{r_{\text{th}}} u + \frac{a^2}{r_{\text{th}}^2} u^2\right) \left(1 + \frac{a^2 - b^2}{r_{\text{th}}^2} u^2 + \frac{2M(sa - b)^2}{r_{\text{th}}^3} u^3\right) (1 - u) \left(1 - \frac{a^2}{r_{\text{th}}^2} u\right)}}. \quad (103)$$

Also, we rewrite the spin as the unit spin $a_{\bullet} \equiv a/M$, and the impact parameter as a unit impact parameter $b_{\bullet} \equiv b/M$ of the light ray. Then the significant different lensing effect by wormholes than black holes is to consider the case that the throat of the wormhole r_{th} is much larger than r_+ characterized by the mass M , which is a horizon scale of Kerr black holes when $\lambda = 0$. So, we expand the integrated function $f_T(u, b_{\bullet})$ in terms of small M/r_{th} as

$$f_T(u, b_{\bullet}) = \frac{b_{\bullet}}{\sqrt{1-u}} \left(\frac{M}{r_{\text{th}}}\right) - \frac{(2sa_{\bullet} - b_{\bullet})u}{\sqrt{1-u}} \left(\frac{M}{r_{\text{th}}}\right)^2 + \mathcal{O}\left(\frac{M}{r_{\text{th}}}\right)^3. \quad (104)$$

It is worth comparing with the case of $r_4 > r_{\text{th}}$ in the next section with a turning point at $r_0 = r_4$ and letting the turning point $r_0 \gg M$. In that case, the above expansion by replacing r_{th} with $r_0 = r_4$ remains the same as the impact parameter obeying (15). For a large r_0 , we know that $b \sim r_0$, giving a constant term in r_0 and other terms of the powers of M/r_0 . After the integration over u , that constant term ends up with π so that the deflection angle (22) is expectedly small in terms of a small value M/r_0 probing the weak field limit that will be discussed later.

In the current case, since (15) is no longer valid, the value of the impact parameter is restricted to $b < b_{\text{th}}$. Ultimately, by integrating the series coefficients, we obtain the expansion of the deflection angle

$$\hat{\alpha}(b_{\bullet}) = -\pi + 4b_{\bullet} \left(\frac{M}{r_{\text{th}}}\right) + \frac{8}{3}(2sa_{\bullet} - b_{\bullet}) \left(\frac{M}{r_{\text{th}}}\right)^2 + \mathcal{O}\left(\frac{M}{r_{\text{th}}}\right)^3. \quad (105)$$

Toward the limit of $r_{\text{th}} > r_4 = r_3$, the impact parameter is $b_{\bullet} = b_{sc}/M$. The expression of the deflection angle looks as if the light rays are reflected back to the light source because of $-\pi$. In fact, we should interpret that light rays are scattered to another spacetime by the throat. The large deflection angle can be visualized as the plot on the middle right in Fig. 6 in [30].

IV. DEFLECTION ANGLE IN THE WEAK DEFLECTION LIMIT

In this section, we are interested in the deflection angle in the other limit, which means that the closest distance r_0 is much larger than the scale of the throat r_{th} and r_+ in the metric characterized the scale of the mass $M \approx M_{\text{WH}}^{(\text{ADM})}$ for λ of order one. The corresponding region is $r_4 \gg r_{\text{th}}$ in Fig. 3. This is in the weak field limit, where the deflection angle is expectedly small, the so-called the weak deflection limit (WDL). Therefore, we choose the ratio $M/r_0 \ll 1$ as a small parameter, and the deflection angle in the WDL can be expressed order by order with respect to this small ratio.

The closest distance r_0 is a turning point of the orbit, that is, the outermost single root r_4 , so light rays will be far from the throat during their journey. Now we first introduce the variable u

$$u \equiv \frac{r_0}{r}, \quad (106)$$

and then the deflection angle can be rewritten as

$$\hat{\alpha} + \pi = 2 \int_0^1 f_W(u, r_0) du, \quad (107)$$

where the integrated function is given by

$$f_W(u, r_0) = \frac{\frac{2Ms_a}{r_0^2}u + \frac{b}{r_0} \left(1 - \frac{2M}{r_0}u\right)}{\sqrt{\left(1 - \frac{2M}{r_0}u + \frac{a^2}{r_0^2}u^2\right) \left(1 + \frac{a^2 - b^2}{r_0^2}u^2 + \frac{2M(sa-b)^2}{r_0^3}u^3\right) \left(1 - \frac{2M(1+\lambda^2)}{r_0}u + \frac{a^2}{r_0^2}u^2\right)}}. \quad (108)$$

The impact parameter $b(r_0)$ for the turning point r_4 is obtained from (15). In terms of the unit spin a_{\bullet} of the wormhole, the expression of $f_W(u, r_0)$ can be written as a function of the

small ratio M/r_0 . We then expand the function $f_W(u, r_0)$ in terms of M/r_0 as

$$\begin{aligned}
& f_W(u, r_0) \\
&= \frac{1}{\sqrt{1-u}\sqrt{1+u}} + \frac{(\lambda^2 + 1)u^2 + (\lambda^2 + 1)u + 1}{\sqrt{1-u}(1+u)^{3/2}} \left(\frac{M}{r_0}\right) \\
&\quad - \frac{a_\bullet^2(1+u)^2(2u^2-1) + 4sa_\bullet(1+u) - 3(\lambda^2+1)^2u^4 - 6(\lambda^2+1)^2u^3 - (3\lambda^4+8\lambda^2+9)u^2 - 2(\lambda^2+3)u - 3}{2\sqrt{1-u}(1+u)^{5/2}} \left(\frac{M}{r_0}\right)^2 \\
&\quad + \mathcal{O}\left(\frac{M}{r_0}\right)^3.
\end{aligned} \tag{109}$$

The integration of $f_W(u, r_0)$ can be carried out by integrating each series coefficient. We obtain the the deflection angle up to the order of $(M/r_0)^2$,

$$\hat{\alpha}(r_0) = 2(\lambda^2 + 2) \left(\frac{M}{r_0}\right) + \left[-4sa_\bullet - 2(\lambda^2 + 2) + \frac{\pi}{4}(3\lambda^4 + 10\lambda^2 + 15)\right] \left(\frac{M}{r_0}\right)^2 + \mathcal{O}\left(\frac{M}{r_0}\right)^3. \tag{110}$$

Finally, let us replace r_0 by b from (14), so the deflection angle in the WDL becomes

$$\hat{\alpha}(b) = 2(\lambda^2 + 2) \left(\frac{M}{b}\right) + \left[\frac{\pi}{4}(3\lambda^4 + 10\lambda^2 + 15) - 4sa_\bullet\right] \left(\frac{M}{b}\right)^2 + \mathcal{O}\left(\frac{M}{b}\right)^3. \tag{111}$$

It might be more transparent to write the deflection angle explicitly in terms of r_{th} (or $r_{\text{th}\bullet} \equiv r_{\text{th}}/M$ normalized by M) as

$$\begin{aligned}
\hat{\alpha}(b) &= \frac{a_\bullet^2 + r_{\text{th}\bullet}(r_{\text{th}\bullet} + 2)}{r_{\text{th}\bullet}} \left(\frac{M}{b}\right) \\
&\quad + \frac{3\pi a_\bullet^4 + 6\pi a_\bullet^2 r_{\text{th}\bullet}^2 + 8\pi a_\bullet^2 r_{\text{th}\bullet} - 64sa_\bullet r_{\text{th}\bullet}^2 + 3\pi r_{\text{th}\bullet}^4 + 8\pi r_{\text{th}\bullet}^3 + 32\pi r_{\text{th}\bullet}^2}{16r_{\text{th}\bullet}^2} \left(\frac{M}{b}\right)^2 + \mathcal{O}\left(\frac{M}{b}\right)^3.
\end{aligned} \tag{112}$$

Then two special limits are considered. In the case of a Kerr black hole by setting the deviation parameter $\lambda = 0$ or the throat $r_{\text{th}\bullet} = r_+/M$, the deflection angle is reduced to

$$\hat{\alpha}(b) = \frac{4M}{b} + \left[\frac{15\pi}{4} - 4sa_\bullet\right] \left(\frac{M}{b}\right)^2 + \mathcal{O}\left(\frac{M}{b}\right)^3, \tag{113}$$

consistent with [19]. When turning off the spin $a = 0$ reducing Schwarzschild-like wormholes, the deflection angle becomes

$$\hat{\alpha}(b) = 2(\lambda^2 + 2) \left(\frac{M}{b}\right) + \left[\frac{\pi}{4}(3\lambda^4 + 10\lambda^2 + 15)\right] \left(\frac{M}{b}\right)^2 + \mathcal{O}\left(\frac{M}{b}\right)^3, \tag{114}$$

which is the same in [25] when the leading order result is considered.

More importantly, we also find that the spin effect of the Kerr-like wormhole will not appear until the order $(M/b)^2$, but the throat effect always exists in each order. In other words, the farther away the light ray is from the wormhole, the more the deflection angle looks like a Schwarzschild-like wormhole. That is different from [26] in the subleading order.

V. RELATIVISTIC IMAGES OF GRAVITATIONAL LENS

In relativistic images, we consider the planar light rays with the lens diagram shown in Fig. 1 when the observers and the light sources are in the same spacetime. The distances between the lens (wormhole) and the light source from the observer are denoted by d_L and d_S whereas d_{LS} represents the distance between the lens and the source. A reference optical axis is defined as the line connecting the observer and the lens so that the angular positions of the source and the image denoted by β and θ , respectively, are measured from the optical axis. The lens equation is given by [13]

$$\tan s\beta = \tan \theta - \frac{d_{LS}}{d_S} [\tan \theta + \tan(\hat{\alpha} - \theta)], \quad (115)$$

where $\hat{\alpha}$ is the deflection angle of light rays obtained from (22) that can also be expressed in terms of the impact parameter b as the light rays approach to the wormhole. In the SDL of our interest, the light rays wind around the wormhole n times, and the deflection angle $\hat{\alpha}$ can be approximately by (23) for the double root or (24) for the triple root. The angle in the lens equation is within 2π and can be obtained from the deflection angle $\hat{\alpha}$ subtracting $2n\pi$.

Together with the relation between the impact parameter b and the angular position of the image given by

$$b = d_L \sin \theta \quad (116)$$

in Fig. 1, we can solve the lens equation (115) with a given angular position of the source β for the angular position of the observed image θ . In the SDL, when the source β is small, θ is expectedly small with the small impact parameter b . Then the lens equation (115) can be further simplified by

$$s\beta \simeq \theta - \frac{d_{LS}}{d_S} [\hat{\alpha}(\theta) - 2n\pi]. \quad (117)$$

In the SDL, we have known that the deflection angle $\hat{\alpha}$ will increase quickly to infinity when the impact parameter approaches to the critical value determined by either the double

or triple root of the radial potential. So we can write the deflection angle as $\hat{\alpha} = 2n\pi + \delta\hat{\alpha}$, where $\delta\hat{\alpha} \ll 2\pi$ means a small angle. That is, there exists an angular position of the image θ_{sn}^0 , such that $\hat{\alpha}(\theta_{sn}^0) = 2n\pi$ serves as the zeroth order solution. Then, we expand the deflection angle around $\theta = \theta_{sn}^0$ as

$$\hat{\alpha}(\theta) = \hat{\alpha}(\theta_{sn}^0) + \hat{\alpha}'(\theta)|_{\theta=\theta_{sn}^0} (\theta - \theta_{sn}^0) + \mathcal{O}(\theta - \theta_{sn}^0)^2. \quad (118)$$

Plugging the expansion into the approximate lens equation (117) to the linear order ($\theta - \theta_{sn}^0$), we have

$$s\beta \simeq \theta_{sn}^0 + \left(1 - \frac{d_{LS}}{d_S} \hat{\alpha}'(\theta_{sn}^0)\right) (\theta - \theta_{sn}^0). \quad (119)$$

Solving for θ , we find the angular position of the image as [16]

$$\theta_{sn} \simeq \theta_{sn}^0 + \left(1 - \frac{d_{LS}}{d_S} \hat{\alpha}'(\theta_{sn}^0)\right)^{-1} (s\beta - \theta_{sn}^0). \quad (120)$$

The deflection angle can have either logarithmic divergence or power-law divergence as the impact parameter approaches to the critical value in the double or triple root of the radial potential. Two cases will be discussed, respectively, in the following. Based on the graphs of the effective potential of Figs. 4 and 5, light rays can possibly pass through the throat to travel from one spacetime to another to be observed. So, when the observers and the light sources are in different spacetime, the light rays pass through the throat to the spacetime of the observers. The images along the line of the sight will be seen. According to [31], due to the symmetry of $l \rightarrow -l$, the light rays from the sources can be mapped into the spacetime of the observers so that the lens equation in (117) in the SDL is assumed to be the same.

A. For the double root: θ_{sn} outside and inside $\theta_{s\infty}$

In the SDL, since the deflection angle in the case of the double root has the logarithmic form as in (23) in [22] with the critical impact parameter b_{sc} for $r_4 = r_3$ or b_{th} for $r_4 = r_{th}$, the angular position of the relativistic image can be approximated as,

$$\theta_{sn} \simeq \theta_{sn}^0 + \frac{e^{(\bar{b}-2n\pi)/\bar{a}} b_{sc/th} d_S}{\bar{a} d_{LS} d_L} (s\beta - \theta_{sn}^0) \quad (121)$$

for $b_{sc/th}/d_L \ll 1$ and with the zeroth order solution

$$\theta_{sn}^0 = \frac{b_{sc/th}}{d_L} \left(1 + e^{\frac{\bar{b}-2n\pi}{\bar{a}}}\right) \quad (122)$$

TABLE I: Relativistic images for the observer/light source in the same spacetime are on the same side of the source with the angular position $\beta = 10$ (μas), where the light rays are along direct orbits seen in Fig. 1 with $\lambda = 0.1 < \lambda_c$ (double root) from (121) and b_{+c} from (28), with $\lambda = \lambda_c$ (triple root) from (126) and b_{+c} from (28), and with $\lambda = 1.2 > \lambda_c$ (double root) from (121) and b_{th} from (15) for the wormhole spin a/M .

a/M	λ	θ_{+1} (μas)	$\hat{\alpha}$	b/M	$\theta_{+\infty}$ (μas)	$\Delta\theta_+$ (μas)
10^{-3}	0.1	26.4250	$2\pi + 32.8104$ (μas)	5.2010	26.3900	0.0350
	0.7067	26.4437	$2\pi + 32.9329$ (μas)	5.2047	26.3900	0.0537
	1.2	32.8007	$2\pi + 45.6084$ (μas)	6.4559	32.2709	0.5298
0.5	0.1	20.9372	$2\pi + 21.8851$ (μas)	4.1209	20.8120	0.1252
	0.4763	20.8400	$2\pi + 21.8037$ (μas)	4.1018	20.8120	0.0280
	1.2	31.0020	$2\pi + 42.0041$ (μas)	6.1019	30.5472	0.4548
0.9	0.1	15.0431	$2\pi + 10.0870$ (μas)	2.9608	14.4517	0.5914
	0.1972	14.4571	$2\pi + 9.3220$ (μas)	2.8455	14.4517	0.0055
	1.2	29.5767	$2\pi + 39.1513$ (μas)	5.8214	29.1486	0.4281

obtained from $\hat{\alpha}(\theta_{sn}^0) = 2n\pi$ for $n = 1, 2, \dots$. The angular position θ_{sn} outside $\theta_{s\infty}$ will decrease when the number of laps n increases, and will approach to $\theta_{s\infty}$ as $n \rightarrow \infty$. The SDL is achieved by $b \rightarrow b_{sc/\text{th}}$ from $b > b_{sc/\text{th}}$. Here, the parameters of the Kerr-like wormhole, the mass M , the spin a , and the throat r_{th} , will be in the expressions of the coefficients \bar{a} , \bar{b} , and the critical impact parameters b_{sc} or b_{th} .

There is another way to approaches to the double roots $r_3 = r_4 = r_{sc}$ and $r_4 = r_{\text{th}}$, that is, $b \rightarrow b_{sc/\text{th}}$ from $b < b_{sc/\text{th}}$ when the observers and the light sources are in different spacetime. The same lens equation from (25) has the zeroth order θ_{sn}^0 solution as

$$\theta_{sn}^0 = \frac{b_{sc/\text{th}}}{d_L} \left(1 + e^{\frac{\bar{b}-2n\pi}{\bar{a}}} \right)^{-1}. \quad (123)$$

The angle of the relativistic image becomes

$$\theta_{sn} \simeq \theta_{sn}^0 - \frac{e^{(\bar{b}-2n\pi)/\bar{a}}}{\bar{a}[1 + e^{(\bar{b}-2n\pi)/\bar{a}}]^2} \frac{b_{sc/\text{th}} d_S}{d_{LS} d_L} (s\beta - \theta_{sn}^0). \quad (124)$$

However, the angular position θ_{sn} inside $\theta_{s\infty}$ will increase when n increases from another spacetime, and will also approach to $\theta_{s\infty}$ when $n \rightarrow \infty$.

TABLE II: Relativistic images for the observers/light sources in the same spacetime are on the opposite side of the source with the angular position $\beta = 10$ (μas), where the light rays are in retrograde orbits seen in Fig. 1 with $\lambda = 0.1 < \lambda_c$ (double root) from (121) and b_{-c} from (28), with $\lambda = \lambda_c$ (triple root) from (126) and b_{-c} from (28), and with $\lambda = 1.2 > \lambda_c$ (double root) from (121) and b_{th} from (15) for the wormhole spin a/M .

a/M	λ	θ_{-1} (μas)	$\hat{\alpha}$	b/M	$\theta_{-\infty}$ (μas)	$\Delta\theta_-$ (μas)
10^{-3}	0.1	26.4451	$2\pi + 72.8586$ (μas)	5.2050	26.4103	0.0348
	0.7075	26.4641	$2\pi + 72.9200$ (μas)	5.2087	26.4103	0.0349
	1.2	32.8081	$2\pi + 85.6189$ (μas)	6.4574	32.2779	0.5302
0.5	0.1	31.2000	$2\pi + 82.4656$ (μas)	6.1409	31.1862	0.0138
	0.8952	31.2673	$2\pi + 82.4924$ (μas)	6.1541	31.1862	0.0811
	1.2	34.8104	$2\pi + 89.6243$ (μas)	6.8515	34.1400	0.6704
0.9	0.1	34.7206	$2\pi + 89.2466$ (μas)	6.8338	34.7131	0.0075
	1.0289	34.8185	$2\pi + 89.5763$ (μas)	6.8531	34.7131	0.1054
	1.2	36.7321	$2\pi + 93.4704$ (μas)	7.2297	35.9030	0.8291

B. For the triple root: θ_{sn} outside and inside $\theta_{s\infty}$

For the triple root, the SDL deflection angle is shown in (24) and has the power-law divergence. The zeroth order solution θ_{sn}^0 is determined by $\hat{\alpha}(\theta_{sn}^0) = 2n\pi$ and from (92) it is obtained as

$$\theta_{sn}^0 = \frac{b_{sc}}{d_L} \left[1 + \left(\frac{2n\pi - \bar{b}}{\bar{a}} \right)^{-4} \right] \quad (125)$$

for $n = 1, 2, \dots$. With the form of the SDL deflection angle in (92), one can solve for θ to find the angular position of the image

$$\theta_{sn} \simeq \theta_{sn}^0 + \frac{4b_{sc}d_S\bar{a}^4}{d_L d_{LS} (2n\pi - \bar{b})^5} (s\beta - \theta_{sn}^0) \quad (126)$$

for $b_{sc}/d_L \ll 1$. Like the double root cases, the angular position θ_{sn} outside $\theta_{s\infty}$ decreases when n increases from $b > b_{sc}$ to approach to the critical value, and also leads to $\theta_{s\infty}$ when $n \rightarrow \infty$. One can approach the triple root from $b < b_{sc}$, which means that the light rays come from another spacetime. Assuming the same lens equation gives

$$\theta_{sn}^0 = \frac{b_{sc}}{d_L} \left[1 + \left(\frac{2n\pi - \bar{b}}{\bar{a}} \right)^{-4} \right]^{-1}. \quad (127)$$

TABLE III: Relativistic images for the observer/light source in different spacetime are on the same side of the source by changing $l \rightarrow -l$ to the same spacetime of the observer with the angular position $\beta = 10$ (μas), where the light rays are along direct orbits seen in Fig. 1 with $\lambda = 0.1 < \lambda_c$ (double root) from (124) and b_{+c} from (28), with $\lambda = \lambda_c$ (triple root) from (128) and b_{+c} from (28), and with $\lambda = 1.2 > \lambda_c$ (double root) from (124) and b_{th} from (15) for the wormhole spin a/M .

a/M	λ	θ_{+1} (μas)	$\hat{\alpha}$	b/M	$\theta_{+\infty}$ (μas)	$\Delta\theta_+$ (μas)
10^{-3}	0.1	25.3624	$2\pi + 30.7245$ (μas)	4.9919	26.3900	-1.0276
	0.7067	26.3364	$2\pi + 32.6869$ (μas)	5.1836	26.3900	-0.0536
	1.2	31.7496	$2\pi + 43.4953$ (μas)	6.2491	32.2709	-0.5212
0.5	0.1	18.1976	$2\pi + 16.3942$ (μas)	3.5817	20.8120	-2.6144
	0.4763	20.7840	$2\pi + 21.5553$ (μas)	4.0908	20.8120	-0.0280
	1.2	30.0990	$2\pi + 40.1985$ (μas)	5.9242	30.5472	-0.4482
0.9	0.1	12.1309	$2\pi + 4.2612$ (μas)	2.3876	14.4517	-2.3208
	0.1972	14.4462	$2\pi + 9.6715$ (μas)	2.8434	14.4517	-0.0055
	1.2	28.7267	$2\pi + 37.4494$ (μas)	5.6541	29.1486	-0.4219

For a given SDL deflection angle in (26), the angular position is obtained as

$$\theta_{sn} \simeq \theta_{sn}^0 - \frac{4b_{sc}d_S\bar{a}^4}{d_L d_{LS}(2n\pi - \bar{b})^5} \left[\left(\frac{2n\pi - \bar{b}}{\bar{a}} \right)^{-4} + 1 \right]^{-2} (s\beta - \theta_{sn}^0) \quad (128)$$

for $b_{sc}/d_L \ll 1$. Again, the angular position θ_{sn} inside $\theta_{s\infty}$ increases as n increases, and approaches to $\theta_{s\infty}$ when $n \rightarrow \infty$.

We now compute the angular positions of the relativistic images of the sources for $n = 1$ ($\theta_{\pm 1}$) by the Kerr-like wormholes with mass $M_{\text{WH}}^{(\text{ADM})} \approx M$, where $M = 4.1 \times 10^6 M_\odot$ and the distance $d_L = 26000$ ly of the scale of the supermassive black hole Sagittarius A* at the center of our Galaxy as an example. We also take the ratio to be $d_{LS}/d_S = 1/2$. In Tables, we consider both the image and the source to be on the same (opposite) sides of the optical axis, where the light rays travel along the direct (retrograde) orbits. The angular positions of the relativistic images are computed by (121). In the case of $b_{sc/\text{th}} \ll d_L$, θ_{sn} is not sensitive to β but is mainly determined by θ_{sn}^0 in (122). In Table I (II), when the observers and the light sources are in the same spacetime, relativistic images on the same (opposite) side of the sources are shown for the outermost and innermost images in the cases of the double root ($r_3 = r_4$) with $\lambda < \lambda_c$, the triple root ($r_3 = r_4 = r_{\text{th}}$) with $\lambda = \lambda_c$, and the double root

TABLE IV: Relativistic images for the observers/ light sources in different spacetime are on the opposite side of the source by changing $l \rightarrow -l$ to the same spacetime of the observers with the angular position $\beta = 10$ (μas), where the light rays are in retrograde orbits seen in Fig. 1 with $\lambda = 0.1 < \lambda_c$ (double root) from (124) and b_{-c} from (28), with $\lambda = \lambda_c$ (triple root) from (128) and b_{-c} from (28), and with $\lambda = 1.2 > \lambda_c$ (double root) from (124) and b_{th} from (15) for the wormhole spin a/M .

a/M	λ	θ_{-1} (μas)	$\hat{\alpha}$	b/M	$\theta_{-\infty}$ (μas)	$\Delta\theta_-$ (μas)
10^{-3}	0.1	25.3870	$2\pi + 70.7760$ (μas)	4.9967	26.4103	-1.0234
	0.7075	26.3567	$2\pi + 72.7245$ (μas)	5.1876	26.4103	-0.0537
	1.2	31.7563	$2\pi + 83.5036$ (μas)	6.2504	32.2779	-0.5216
0.5	0.1	30.9951	$2\pi + 81.9871$ (μas)	6.1005	31.1862	-0.1911
	0.8952	31.1053	$2\pi + 82.2747$ (μas)	6.1222	31.1862	-0.0809
	1.2	33.4825	$2\pi + 86.9603$ (μas)	6.5901	34.1400	-0.6575
0.9	0.1	34.7087	$2\pi + 89.0440$ (μas)	6.8315	34.7131	-0.0043
	1.0289	34.6079	$2\pi + 89.2774$ (μas)	6.8116	34.7131	-0.1051
	1.2	35.0926	$2\pi + 90.1820$ (μas)	6.9070	35.9030	-0.8104

($r_4 = r_{\text{th}}$) for $\lambda > \lambda_c$. Apart from the fact that the images are distributed with respect to the reference line connecting the wormhole and the observer is in an asymmetric way, another common trend is that the angular position decreases (increases) in the wormhole spin a for the direct (retrograde) orbits, which is also found in Table III (IV), when the light sources are from another spacetime. Notice that since $b \approx d_L\theta$, for $b > b_c$ (for $b < b_c$), θ decreases (increases) from θ_1 to θ_∞ . As can be seen from the angular positions in the Tables, given a spin a , in the cases of the double roots as λ increases with λ_c is excluded for the triple root, we observe a significant increase in the direct angular position θ_{+1} in Table I, especially in the case of the near extreme Kerr-like wormhole $a \rightarrow M$. In contrast, the increase in the retrograde angular position θ_{-1} in Table II is less noticeable. In fact, this is consistent with Fig. 3 in [27] in the study the shadow of the nonspherically symmetric wormholes.

VI. SUMMARY AND OUTLOOK

In this paper, we study the strong gravitational lensing by Kerr-like wormholes with an additional parameter λ to specify the location of the throat. The corresponding radial potential is derived from the motion of the light rays along the coordinate r with four roots given by the mass and spin of the wormholes and the light ray impact parameter of the equatorial orbits and the other two roots from the throat and the other associated root. We classify the roots by finding the parameter space diagram of the impact parameter of light rays and the parameter λ of the throat, where the throat together with other roots become either double or triple root, potentially giving the divergence of the deflection angle of the light rays in the SDL. In addition, the effective potential in terms of the proper distance from the throat is constructed with which to realize how the light rays can either travel within one spacetime, where the observers are in the same spacetime or through the throat to another spacetime which the observers reside in. In particular, when the observer and light sources are in different spacetimes. The deflection angle can still be defined using the symmetry of the proper distance $l \rightarrow -l$, mapping the light rays from the sources to the same spacetime of the observers, where the corresponding detailed trajectories can be seen in the embedded diagram in [30], which shares the same gravitational lens equation in the cases of both observers and light sources in the same spacetime. In general, while the logarithmic divergence is known as the double root are approached, the stronger power-law (non-logarithmic) divergence is found for the triple root cases. The observational effects such as relativistic images due to the light deflection by wormholes are discussed. In the future, the most prompt work for us is to follow [30] and find the trajectories of light rays, perhaps analytically.

Appendix A: Roots of the radial potential

The radial potential $R(r)$ of the Kerr black holes on the equatorial plane can be rewritten as a quartic function

$$R(r) = r^4 + Ur^2 + Vr \tag{A1}$$

with the coefficient functions given by

$$U = a^2 - b^2, \quad (\text{A2})$$

$$V = 2M(b_s - a)^2. \quad (\text{A3})$$

There are four roots, namely $R(r) = (r - r_1)(r - r_2)(r - r_3)(r - r_4)$ with the property $r_1 + r_2 + r_3 + r_4 = 0$ and $r_1 < r_2 < r_3 < r_4$, and can be written as [32]

$$r_1 = -z - \sqrt{-\frac{U}{2} - z^2 + \frac{V}{4z}}, \quad (\text{A4})$$

$$r_2 = -z + \sqrt{-\frac{U}{2} - z^2 + \frac{V}{4z}}, \quad (\text{A5})$$

$$r_3 = +z - \sqrt{-\frac{U}{2} - z^2 - \frac{V}{4z}}, \quad (\text{A6})$$

$$r_4 = +z + \sqrt{-\frac{U}{2} - z^2 - \frac{V}{4z}}. \quad (\text{A7})$$

The following notation has been used,

$$z = \sqrt{\frac{\Omega_+ + \Omega_- - \frac{U}{3}}{2}}, \quad \Omega_{\pm} = \sqrt[3]{-\frac{\varkappa}{2} \pm \sqrt{\left(\frac{\varpi}{3}\right)^3 + \left(\frac{\varkappa}{2}\right)^2}}, \quad (\text{A8})$$

where

$$\varpi = -\frac{U^2}{12} - W, \quad \varkappa = -\frac{U}{3} \left[\left(\frac{U}{6}\right)^2 - W \right] - \frac{V^2}{8}. \quad (\text{A9})$$

Apparently, using the above formulas gives $r_2 = 0$ as anticipated.

Acknowledgments

This work was supported in part by the Ministry of Science and Technology, Taiwan, under Grant No.109-2112-M-259-003.

-
- [1] C. W. Misner, K. S. Thorne, J. A. Wheeler, and S. Chandrasekhar, *Physics Today* **27**, 47 (1974), URL <https://doi.org/10.1063/1.3128805>.
- [2] A. Einstein and N. Rosen, *Phys. Rev.* **48**, 73 (1935), URL <https://doi.org/10.1103/physrev.48.73>.

- [3] J. A. Wheeler, Phys. Rev. **97**, 511 (1955), URL <https://doi.org/10.1103/physrev.97.511>.
- [4] J. A. Wheeler, Geometrodynamics (1962).
- [5] M. S. Morris, K. S. Thorne, and U. Yurtsever, Phys. Rev. Lett **61**, 1446 (1988), URL <https://doi.org/10.1103/physrevlett.61.1446>.
- [6] M. Visser, Lorentzian wormholes (American Institute of Physics, 1995).
- [7] B. P. Abbott *et al.* (LIGO Scientific Collaboration and Virgo Collaboration), Phys. Rev. Lett **116**, 061102 (2016), URL <https://doi.org/10.1103/physrevlett.116.061102>.
- [8] B. P. Abbott *et al.* (LIGO Scientific Collaboration and Virgo Collaboration), Phys. Rev. X **9**, 031040 (2019), URL <https://doi.org/10.1103/physrevx.9.031040>.
- [9] R. Abbott *et al.* (LIGO Scientific Collaboration and Virgo Collaboration), Phys. Rev. X **11**, 021053 (2021), URL <https://doi.org/10.1103/physrevx.11.021053>.
- [10] The Event Horizon Telescope Collaboration *et al.*, The Astrophysical Journal Letters **875**, L1 (2019), URL <https://doi.org/10.3847/2041-8213/ab0ec7>.
- [11] The Event Horizon Telescope Collaboration *et al.*, The Astrophysical Journal Letters **930**, L12 (2022), URL <https://doi.org/10.3847/2041-8213/ac6674>.
- [12] J. B. Hartle, Gravity: An Introduction to Einstein's General Relativity (Benjamin Cummings, 2003).
- [13] K. S. Virbhadra and G. F. R. Ellis, Phys. Rev. D. **62**, 084003 (2000), URL <https://doi.org/10.1103/physrevd.62.084003>.
- [14] S. Frittelli, T. P. Kling, and E. T. Newman, Phys. Rev. D. **61**, 064021 (2000), URL <https://doi.org/10.1103/physrevd.61.064021>.
- [15] V. Bozza, S. Capozziello, G. Iovane, and G. Scarpetta, General Relativity and Gravitation **33**, 1535 (2001), URL <https://doi.org/10.1023/a:1012292927358>.
- [16] V. Bozza, Phys. Rev. D. **66**, 103001 (2002), URL <https://doi.org/10.1103/physrevd.66.103001>.
- [17] E. F. Eiroa, G. E. Romero, and D. F. Torres, Phys. Rev. D. **66**, 024010 (2002), URL <https://doi.org/10.1103/physrevd.66.024010>.
- [18] S. V. Iyer and A. O. Petters, General Relativity and Gravitation **39**, 1563 (2007), URL <https://doi.org/10.1007/s10714-007-0481-8>.
- [19] S. V. Iyer and E. C. Hansen, arXiv: 0908.0085 (2009), URL <https://arxiv.org/abs/0908.0085>.

- [20] N. Tsukamoto, Phys. Rev. D **95**, 064035 (2017), URL <https://doi.org/10.1103/physrevd.95.064035>.
- [21] Y.-W. Hsiao, D.-S. Lee, and C.-Y. Lin, Phys. Rev. D **101**, 064070 (2020), URL <https://doi.org/10.1103/physrevd.101.064070>.
- [22] T. Hsieh, D.-S. Lee, and C.-Y. Lin, Phys. Rev. D **103**, 104063 (2021), URL <https://doi.org/10.1103/physrevd.103.104063>.
- [23] T. Hsieh, D.-S. Lee, and C.-Y. Lin, Phys. Rev. D **104**, 104013 (2021), URL <https://doi.org/10.1103/physrevd.104.104013>.
- [24] T. Damour and S. N. Solodukhin, Phys. Rev. D. **76**, 024016 (2007), URL <https://doi.org/10.1103/physrevd.76.024016>.
- [25] N. Tsukamoto, Phys. Rev. D **101**, 104021 (2020), URL <https://doi.org/10.1103/physrevd.101.104021>.
- [26] A. Övgün, Phys. Rev. D **98**, 044033 (2018), URL <https://doi.org/10.1103/physrevd.98.044033>.
- [27] S. Kasuya and M. Kobayashi, Phys. Rev. D **103**, 104050 (2021), URL <https://doi.org/10.1103/physrevd.103.104050>.
- [28] P. Bueno, P. A. Cano, F. Goelen, T. Hertog, and B. Vercoe, Phys. Rev. D **97**, 024040 (2018), URL <https://doi.org/10.1103/physrevd.97.024040>.
- [29] M. Amir, K. Jusufi, A. Banerjee, and S. Hansraj, Classical and Quantum Gravity **36**, 215007 (2019), URL <https://doi.org/10.1088/1361-6382/ab42be>.
- [30] P. Taylor, Phys. Rev. D. **90**, 024057 (2014), URL <https://doi.org/10.1103/physrevd.90.024057>.
- [31] R. Shaikh, P. Banerjee, S. Paul, and T. Sarkar, Journal of Cosmology and Astroparticle Physics **2019**, 028 (2019), URL <https://doi.org/10.1088/1475-7516/2019/07/028>.
- [32] C.-Y. Wang, D.-S. Lee, and C.-Y. Lin, Phys. Rev. D **106**, 084048 (2022), URL <https://doi.org/10.1103/physrevd.106.084048>.
- [33] S. Chandrasekhar, The Mathematical theory of black holes (Oxford University Press, 1998).